METAL SPIN LATTICE RELAXATION MECHANISMS IN LIQUID MOLYBDENUM AND TUNGSTEN HEXAFLUORIDES AND P.M.R. STUDY OF DEUTERATED AMMONIUM IONS

by

STEPHEN ANTHONY BROOKS

B. Sc. (Hons.)

University of Manitoba, 1967

A DISSERTATION SUBMITTED IN PARTIAL FULFILLMENT

OF THE REQUIREMENTS FOR THE DEGREE OF

MASTER OF SCIENCE

in the Department

of

Chemistry

Simon Fraser University

February 1969

EXAMINING COMMITTEE APPROVAL

E. J. Wells
Senior Supervisor

S. K. Lower
Examining Committee

D. Meakin
Examining Committee

To My Parents.

MEMORANDUM

To the Student:-

The time has come, the supervisor said,
To talk of many things,
Of Physics and N.M.R. and Relaxation,
Of Chemical Shifts and Things.

ACKNOWLEDGEMENT

The author expresses sincere thanks and gratitude to Professor E. J. Wells for his many constructive criticisms and stimulating discussions during the period that this research was being carried out.

Thanks are in order for Dr. J. Hallett whose advice on experimental technique so often proved useful.

The author wishes to thank Professor G. Malli, Dr. M. Kaplansky and Mr. S. O. Chan for their valuable suggestions and advice.

The assistance of Mr. A. M. Cutteridge and Mr. D. Robinson in the construction of the glass apparatus is also gratefully acknowledged.

The author is indebted to the Chemistry Department of Simon Fraser University for financial support.

ABSTRACT

The recent work of Rigny and Virlet on F^{19} spin lattice relaxation processes in liquid MoF_6 has been extended by a study of the spin relaxation mechanisms of the magnetic metal nuclei at the centre of these uncharged octohedral species. T_1 Relaxation transitions among the Zeeman manifold of the nuclei Mo^{97}, Mo^{95} and W^{183} are reflected as T_2 mechanisms on the spin-coupled F^{19} nuclei in MoF_6 and WF_6 respectively, and thus can be studied by high resolution F^{19} spectroscopy over the available liquid range.

From a detailed study of the temperature dependences of the line widths of the F^{19} sextets due to Mo^{97} and Mo^{95}, together with a consideration of the Mo transition probabilities under the usual mechanisms, we conclude that in octohedral MoF_6, the Mo^{97} nuclei relax by quadrupolar coupling with instantaneous field gradients produced by intermolecular collision, with an activation energy of (1.4 ± 0.2) Kcals moles^{-1}. However Mo^{95} nuclei, with smaller quadrupolar moments, relax predominantly by modulation of intramolecular spin-rotation interaction, with activation energy (2.2 ± 0.3) Kcals mole^{-1}. No evidence was found for Mo^{95} relaxation by higher order (octopole, etc.) interactions. An activation energy of 1.6 Kcals mole^{-1} had been measured previously for the F^{19} spin-rotation process in MoF_6; the

different values obtained for the various processes in this liquid presumably represent a breakdown of the microscopic rotational diffusion model.

A similar study of spin $\frac{1}{2}$ W^{183} from F^{19} data on liquid WF_6 gave results consistent with spin-rotation interaction for the dominant mechanism, with an activation energy of (3.4 ± 1.1) Kcals $mole^{-1}$. However, in this case the effects of W^{183} relaxation on the F^{19} spectra are small and largely obscured by instrumental inhomogeneities. The spin-rotation interaction constant at W^{183} in WF_6 is apparently smaller than the spin-rotation constant at the Mo^{95}, a remarkable behaviour parallel to the F^{19} interaction constants in the two molecules, and ascribed to the filled 4f shell between Mo and W.

An attempt was made to study N^{14} relaxation by Rotary Echo experiments on the H^1 spectra in aqueous solutions of ammonium ions. This proved instrumentally impractical due to the short H^1 T_1 values. However, in the course of this work it was found possible to prepare solutions of deuterated ammonium ions with varying ratios of the deuterated components, and hence to study the successive deuterium isotope effects on the proton chemical shifts and the coupling constants. J_{NH} was found to decrease slightly with deuteration and J_{HND} to increase; both trends can be explained as a reduction in the N-D bending vibration amplitude against N-H.

The observed low field proton shift on successive deuteration through $\overset{+}{N}H_4$, $\overset{+}{N}H_3D$, $\overset{+}{N}H_2D_2$, $\overset{+}{N}HD_3$, an effect opposite to that described in the deuterated methanes, can be accounted for in terms of an increase in the strength of the ion-solvent hydrogen bond on deuteration.

TABLE OF CONTENTS

PART B

LIST OF TABLES

LIST OF FIGURES

CHAPTER I

INTRODUCTION

.... pale, deluding beams. (Dido and Aneus)

(1) Historical

Faraday's discoveries in electromagnetism led Maxwell to predict and later Hertz to discover radiowaves. Faraday's experiments in electrolysis revealed the quantization of electrical charge and the electrical aspects of matter which are responsible for the interaction of these radiowaves with material particles. Faraday's ice-pail experiments presaged the invention of microwave cavities and wave guide. It was Faraday's search for a common denominator for all physical manifestations which led him to his discoveries of basic relations between electricity and magnetism, between electricity and matter and between magnetism and light. Thus Faraday's work led to the development of the implements or tools of microwave and radio-frequency spectroscopy (1).

It was Rutherford, who in 1910 directed his students Marsden and Geiger to pass a beam of particles through a thin metal-foil, the deflections of the particles being observed on a zinc sulphide screen. From this experiment on α-particle scattering Ernest Rutherford in 1911 suggested the nuclear model of the atom (2).

In 1924 W. Pauli suggested that the hyperfine structure in atomic spectra might be explained by a small magnetic moment of the nucleus (3)(4). The interaction of this magnetic dipole with the motion of the electrons would produce a hyperfine multiplet in a similar way as a multiplet is produced by the interaction of the intrinsic magnetic moment of the electron with the orbital motion. The introduction of the electronic spin, by Uhlenbeck and Goudsmit in 1925, made it possible to explain many hitherto mysterious details of the spectra.

It appeared appropriate to connect the magnetic moment of the nuclei with rotating charges and to attribute to the nucleus a mechanical spin. The evidence for the nuclear spin and nuclear magnetic moment is now manyfold and the concept of the spinning nucleus must be considered to be as well-founded as that of the spinning electron. Bloembergen (3) points out several experimental techniques that might be performed to determine nuclear spin, as well as the magnitude of the magnetic moment.

In 1935 H. Schuler and T. Schmidt (3)(5) observed deviations in the interval rule in the hyperfine multiplets of Europium, explained by assuming another interaction between the nucleus and the surrounding electrons via the nuclear electric quadrupole moment. Since then it has been shown (6) that for spins larger than $\frac{1}{2}$ there can be the presence of an

electric quadrupole. In general by knowing the spin, I, of a nucleus one can apply a 2^{2I} rule to obtain the size of the respective nuclear multipole, remembering alternation in magnetic and electric characters.

Further stimulus for the investigation between the nuclear electric moments and their environments was stimulated by R. V. Pound's theoretical work (6)(7) and in H. Delmelt and H. Kruger's experimental work (8) on the interaction of nuclear quadrupolar moments in liquids and solids. In 1955 T. Wang (9) postulated that an unexplained shift in the pure quadrupole spectrum of Sb^{121} and Sb^{123} was due to the static interaction of the nuclear electric hexadecapole interaction. In 1966, the interaction of the electric hexadecapole moment with externally added phonons was postulated to be the cause of the observed $\Delta M = \pm 3$ In^{115} transitions in InAs (10, 11). It was further pointed out in 1967 by H. P. Mahon (12) that the hexadecapole transition probability in terms of the quadrupolar transition probability is

$$P_h \approx 10^{-9} P_q$$

(ii) <u>Relaxation of Nuclear Spins in Diamagnetic Liquids</u>

In a spin system consisting of two spin $\frac{1}{2}$ nuclei placed in a constant magnetic field H_o, the magnetic moment of nucleus 1 creates a certain additional magnetic field H_1 in the region where nucleus 2 is located. Due to collisions with

other molecules of the sample, the nucleus under consideration will change its position and thereby vary the field H_1 with time; as a result, transitions between the different magnetic energy levels of nucleus 2 will be induced. In this manner the magnetic dipole-dipole interaction between the spins of 1 and 2, modulated by the motion of the molecule leads to a process for the attainment of thermal equilibrium between the spin system and the thermal molecular motion (13).

In a similar manner for spins larger than $\frac{1}{2}$, thermal equilibrium is attained, either by the coupling of the electric field gradients arising from the asymmetry of the molecular charge distribution with the nuclear quadrupole moment (3), or by the distortion of a sperical electron cloud due to intermolecular collisions and subsequent coupling to the nuclear quadrupole moment.

P. S. Hubbard (14) gave a general theoretical treatment of the effects of the spin-rotational interaction on the nuclear spin-lattice relaxation time, using as a model a spherical top in which were embedded equivalent nuclei which interacted with the molecular rotation through an axially symmetric tensor. P. W. Atkins (15) extended Hubbard's results to admit the possibility of an interaction tensor that was fully anisotropic for molecules undergoing anisotropic rotational diffusion. M. Bloom (16) and H. Gutowsky (17), in addition to many other workers, have applied this mechanism

to explain the experimental results of the deutero-and halo-methanes respectively.

Another relaxation mechanism which is time dependent, as a result of frequent collisions in fluids, is due to the random modulation of chemical shift anisotropy leading to spin lattice equilibration and can thus be separated from spin-rotational effects through the dependence of $\underline{\underline{\sigma}}$ and thus T_1 on the H_o field strength (18 p. 316).

Summarizing, one can group the preceeding mechanisms into inter- and intra- molecular interactions (19). Within the intra-molecular interaction one can associate

(a) dipole-dipole interactions ($I \cdot I$)
(b) electric quadrupolar interactions (e^2qQ)
(c) Spin-rotational interactions ($I \cdot \underline{C} \cdot J$)
(d) Chemical shift anisotropy ($\underline{\underline{\sigma}}$)
(e) Higher order nuclear multipole interactions.

Within the intermolecular interaction one may group:

(a) dipole-dipole ($I \cdot I$)
(b) electric quadrupole interaction (e^2qQ) (due to distortion of the spherical tensor).

The above interactions are useful in that they give information on the random motion of fluids and follow directly from the pioneering work of N. Bloembergen, E. Purcell and R. Pound in 1948 (7).

(iii) Thesis Format

This thesis is divided into parts A and B. In part A, which constitutes the major portion of the thesis and with which this introduction is closely linked, the relaxation

mechanisms occurring in liquid molybdenum and tungsten hexafluorides are considered by studying the temperature dependence of the resulting high resolution F^{19} N.M.R. spectra at 56.4 Mhz.

A theoretical study of relaxation mechanisms is outlined in Chapter II, following closely the approach of Abragam (18) to obtain the relevant transition probabilities between the Zeeman spin states of the central metal nucleus, allowing one to obtain information on the line shapes of the observed spin coupled nuclei.

The dominant Mo mechanisms found in MoF_6 were quadrupolar (Mo^{97}) and spin rotational interaction (Mo^{95}). The data for the W^{183} mechanism in WF_6 is consistent with the spin rotation interaction. The conclusions for associating the above mechanisms with the various magnetic isotopes of Mo and W were obtained by interpreting the results obtained from the temperature dependence of the F^{19} spectra (Chapter III) and using the theory of Chapter II assuming a slow relaxation limit (i.e., $R_{1M} \ll 2\pi J_{M-F}$).

In part B there appears an explanation of the observed increase in J_{D-N-H} or decrease in J_{N-H}, as well as the downfield proton shift noted with successive deuterations of the ammonium ion in solutions of ammonium nitrate, as obtained from the H^1 N.M.R. spectra.

CHAPTER II

THEORY

Fugit irreparabile tempus

(1) General Relaxation

A system of nuclear spins, I, with magnetic moments, $\gamma\hbar I$, has, at equilibrium in a magnetic field H_0, a magnetization given by Curie's Law:

$$M_0 = \frac{\gamma^2 \hbar^2 I(I+1)}{3k} \frac{H_0}{T} \qquad (1)$$

where M_0 is the magnetization associated with a field H_0, and where γ is the magnetogyric ratio of the nucleus of nuclear spin I. $\hbar = \frac{h}{2\pi}$, k, T are Plank's constant divided by 2π, Boltzmann's constant and temperature in degrees Kelvin respectively.

Equation (1) is approached under normal circumstances by a first-order rate process with rate constant $R_1 = 1/T_1$ where

$$d/dt \ln (\langle M_z \rangle - M_0) = - 1/T_1 \qquad (2)$$

where $\langle M_z \rangle$ is the average magnetization in the z direction. The transverse components M_x and M_y likewise approach their equilibrium values of zero by another rate process, characterised by a time scale T_2.

The average magnetization, $\langle M_z \rangle$, can be removed from equilibrium and its subsequent return followed by a number of experimental means, many of which are summarized in Abragam (18) and Slichter (20).

In discussing relaxation processes two points can be

made; firstly, nuclear relaxation in liquids is generally governed by interactions having a distance scale of molecular dimensions, so that the dynamical processes responsible for bulk transport phenomena can be studied on a molecular level. Secondly, the use of N.M.R. as a tool for such studies is characterised by the fact that the time scale for such processes responsible for nuclear relaxation, (i e. of the order of the larmor period, 10^{-8} sec.), is much longer than the time scale of random motions of individual small molecules (10^{-10} - 10^{-13} sec.). (21)

Since the Hamiltonian, $\mathcal{H}_1(t)$, for the relaxation process is a function of time, knowledge of how this Hamiltonian at one time is correlated to its value at a later time is gained from the auto-correlation function, and in such spin interactions as dipole-dipole, normal electric quadrupole and chemical anisotropy, the associated correlation functions involve angles through second rank spherical harmonics e.g.

$$Y(\tau) = \langle Y_{20}(t)\ Y_{20}(t + \tau)\rangle \qquad (3)$$

whereas for the spin-rotational interaction the correlation function involves components of angular momentum e.g.

$$G(\tau) = \langle J_z(t)\ J_z(t + \tau)\rangle \qquad (4)$$

where $Y(\tau)$ and $G(\tau)$ are the respective correlation functions. The characteristic times τ_θ and τ_φ for the loss of these two types of correlation may be quite different, and the relation between them depends sensitively on the type of

(rotational) random process involved. This is analogous to a classical rotational random walk consisting of short free rotations interrupted by hard collisions (21). The angular momentum is completely changed in every collision so that τ_G is very short. However, if the mean rotation angle $\bar{\theta}$ between collisions is very small many steps of the random walk are required to accumulate a sensible change in orientation and τ_θ is long. By comparing τ_G and τ_θ it ought to be possible to learn something about $\bar{\theta}$ i.e. about where the random walk lies between the hydrodynamic Debye limit $\tau_G \ll \tau_\theta$, $\tau_G\ \tau_\theta$ = constant, and the gas-like limit $\tau_G \sim \tau_\theta$, $\bar{\theta} > 2\pi$.

Departures from the hydrodynamic limit were first noted by Gutowsky et al (22), (17), who observed that above a certain temperature in liquid CHF_3 the 'normal' rise of T_1 with temperature (arising from the shortening τ_θ) was reversed owing to a lengthening of τ_G and hence the progressive dominance of the spin-rotational interaction.

In special cases T_1 can be measured for two different spins attached to the same nuclear framework (23), the nuclear relaxation process of one nuclear species may be controlled by an angle dependent correlation function τ_θ, above, while the other nuclear species may be dominated by an angular momentum correlation function τ_G.

In this chapter the transition probabilites of the nuclear spin relaxation mechanisms mentioned in Chapter I

shall be considered with reference to Appendix 1.

(2) Intramolecular Dipole-Dipole Interaction

In the approximation of rigid molecules the time dependence of the internal dipole-dipole coupling of the nuclei comes via re-orientation of the molecule. The Hamiltonian, in the laboratory frame, is given by Equation (1) of Appendix 1, where the $F^{(q)}(t)$ are lattice operators defined by

$$F_{ij}^{(q)}(t) = \left(\frac{3\pi}{10}\right)^{1/2} \gamma^2 \hbar \vec{r}_{ij}^{-3} (-1)^k Y_2^{-k} (\theta_{ij}, \phi_{ij}) \quad (5)$$

where the Y_2^k are normalised second-rank spherical harmonics, $\vec{r}_{ij}$ is the radius vector from the i^{th} to j^{th} nucleus and the polar angles specifying the direction of $\vec{r}_{ij}$ in the laboratory co-ordinate system are denoted by θ_{ij} and ϕ_{ij}. From equation (2) of Appendix 1 it is possible to show that:

$$P_{M,\, M\pm1}(I) = n\, \gamma_I^2\, \gamma_S^2\, \hbar^2\, S(S+1) \cdot \frac{4}{3b^6}\, \tau_\theta \left| \langle M | I_\mp | M \pm 1 \rangle \right|^2 \quad (6)$$

where n is the number of equivalent heteronuclear spins S, assumed independent, each at a distance b from the considered I spin, assuming extreme narrowing with respect to the orientational correlation time τ_θ and neglecting cross-relaxation effects. (18)

(3) Intermolecular Dipole-Dipole Interaction

Similarly, the I-spin transitions induced by unlike S-spins in neighbouring molecules under the intermolecular translation can be shown to be: (18)

$$P_{M,\ M\pm1}(I) = \gamma_I^2\gamma_s^2\hbar^2\ S(S+1).\ \frac{16\pi}{75}\frac{\nu}{a^6}\ \tau_\theta\left|\langle M\left|I_\mp\right|M\pm1\rangle\right|^2 \qquad (7)$$

where a is the distance of closest approach between the I-spin considered and a neighbouring S-spin.

(4) Anisotropic Shielding

The Hamiltonian for anisotropic shielding can be written (24)

$$\mathcal{H}'(t) = \sum_i \gamma_i \vec{I}(i).\ \underline{\underline{\sigma}}_i(t).\vec{H}_o \qquad (8)$$

where $\underline{\underline{\sigma}}_i(t)$ is the traceless part of the shielding tensor written in the laboratory frame and $\vec{H}_o = H_o\vec{k}$ is the applied d.c. field. The time dependence of the tensor $\underline{\underline{\sigma}}_i(t)$ enters through random molecular reorientation. From equation (2) of Appendix 2 it is possible to show that

$$P_{M,\ M\pm1} = \frac{6}{40}\gamma_I^2\ H_o^2\ (\sigma_z)^2\ \tau_\theta\left|\langle M\left|I_\mp\right|M\pm1\rangle\right|^2 \qquad (9)$$

where σ_z is the component of the chemical shift tensor in the molecular frame.

(5) Spin-Rotation Interaction

The perturbation Hamiltonian for spin I under spin-rotational interaction can be written (24)

$$\mathcal{H}'(t) = \gamma_I\ \vec{I}\cdot\underline{\underline{C}}\cdot\vec{J}(t) \qquad (10)$$

where $\vec{J}(t)$ is the instantaneous angular momentum of the molecule, $\underline{\underline{C}}$ is the spin-rotation interaction tensor for nucleus I in the molecular frame.

An expression for the autocorrelation function, equation (4) Appendix 1, for this interaction is found to be:

$$G(\tau) = 1/4\ C^2\ \overline{J_+(0) \cdot J_-(\tau)}$$

$$= 1/4\ C^2\ J_+(0)\ J_-(0)\ e^{i\omega_J \tau} e^{-\tau/\tau_G}$$

(where $J_-(\tau) = J_-(0) e^{i\omega_J \tau} e^{-\tau/\tau_G}$ for $\tau_G \equiv T_2$ of the J vector)

$$\approx \frac{C^2}{6} J(J+1)\ e^{i\omega_J \tau}\ e^{-\tau/\tau_G}$$

Since by symmetry $\mathcal{J}(\omega_I) = 2\int_0^a g(\tau) e^{-i\omega_J \tau}$

then $\mathcal{J}(\omega_I) \approx \frac{C^2}{3} J^2\ \tau_G^2$

for $J^2 >> J$ and $\tau_G << 1$, for the spin-rotation interaction coefficient. From equation (2) of Appendix 1 it is possible to write the transition probability for this interaction as

$$P_{M,\ M\pm1} = 1/3\ C^2\ J^2\ \tau_G\ |\langle M\ |\ I_{\mp}\ |\ M\pm1\rangle| \qquad (11)$$

for the special case of a spherically symmetric molecule. Equation (11) can be simplified by applying classical mechanics, i. e.

$$E_{rot} = \frac{J^2 \hbar^2}{2I} = \frac{3}{2}\ kT \text{ for } J^2 >> J$$

and $\tau_G << 1$.

$$J^2 = 3IkT/\hbar^2 \qquad (12)$$

Substituting for J^2 from (12) into (11)

$$P_{M,\, M\pm1} = \frac{C^2\, I\, k\, T}{\hbar^2}\, \tau_G \left| \langle M \mid I_{\mp} \mid M\pm1 \rangle \right|^2 \qquad (13)$$

(6) Nuclear Quadrupole Interaction

Quadrupole relaxation at the central nucleus of a molecule which is octohedral when isolated implies a lowering of the molecular symmetry in the liquid. Two mechanisms have been considered:

(a) Nuclear centrifugal distortion due to molecular rotation.

(b) Electronic distortion due to intermolecular collisions.

(a) In considering the effect of centrifugal distortion reference is made to a similar effect in diatomic molecules (Banwell p. 42 (25)).

i.e. $\epsilon_J = B\, J(J+1) - D\, J^2(J+1)^2 \ cm^{-1}$ (14)

where $\epsilon_J = E_J/hc$, for E_J the energy of rotation and c the speed of light and where B, the rotational constant is defined as

$$B = h/8\pi^2 I_B c$$

where I_B is the moment of inertia associated with rotation. D is the centrifugal distortion constant, where

$$D = \frac{h^3}{32\pi^4\ I^2\gamma^2 kc} = \frac{4B^3}{\bar{\omega}^2}$$

Hence it is possible to define

$$B_J = B_e \left[1 - \frac{4 B_e^2}{\bar{\omega}^2} \cdot J(J+1)\right] = \frac{h}{8\pi^2 \mu r_J^2 c} \qquad (15)$$

$$= B_e [1 - \epsilon]$$

where $\epsilon = \frac{4 B_e^2}{\bar{\omega}^2} J(J+1)$

Hence from (15) $B_J \alpha 1/r^2$ and by performing a power series expansion

$$r_J \approx r_e[1 + 1/2\ \epsilon] \qquad (16)$$

(b) Another means of disrupting the molecular symmetry is via intermolecular collisions, causing a distortion of the electron cloud surrounding the nucleus thus generating a field gradient which interacts with a nuclear quadrupolar moment. However, the field gradient $q(\theta,t)$ observed in such a situation fluctuates with the kinetic energy of collision, unlike the case considered by Abragam (18), where q is constant to first order in the molecular frame.

Due to this fluctuating field gradient an efficient quadrupolar relaxation is possible. This being the case the correlation function associated with such an anisotropic interaction, Equation (3), may be used for the equilibrium ensemble average. Here the argument of Y is the angle θ between the collision vector and $H_o\vec{k}$, the d.c. field and if the two body collision process is Markovian in direction, then

$$\langle Y_{20}(t)\ Y_{20}(t+\tau)\rangle = \langle |Y_{20}(0)|^2 \rangle \exp(-t/\tau_\theta) \qquad (17)$$

where τ_θ is the correlation time for the molecular collision vector. Since equation (17) is a function of $\bar{\theta}$ it is possible to apply Abragam's theory (18), for which he shows that the transition probability may be written

$$P_{M,\ M\pm1} = \frac{3}{80}\left[\frac{eqQ}{\hbar}\frac{1}{I(2I-1)}\right]^2 \tau_\theta \left|\langle M| I_{\mp} I_Z + I_Z I_{\mp} |M \pm 1\rangle\right|^2$$

$$P_{M,\ M\pm2} = \frac{3}{80}\left[\frac{eqQ}{\hbar}\frac{1}{I(2I-1)}\right]^2 \tau_\theta \left|\langle M| I_{\mp}^2 |M \pm 2\rangle\right|^2 \qquad (18)$$

and since the matrix elements of I_Z, which is diagonal, are represented by:

$$I_Z\ \Phi(I, M) = M\ \Phi(I, M)$$

If the $\Phi(I, M)$ are normalized, then it follows that

$$(\phi(I'M'),\ I_Z\ \phi(I, M)) = \langle I'M'|\ I_Z|\ I_M\rangle$$

$$= M\ \delta_{MM'}\ \delta_{II'} \qquad (19)$$

$$I_- I_+\ \phi(I, M) = (I^2 - I_Z^2 - I_Z)\ \Phi(I, M)$$

$$= (I(I+1) - M(M+1))\ \Phi(I, M) \qquad (20)$$

Expanding the terms in brackets in Equations (18) separately and operating on them gives

$$|\langle M|\ I_+^2|\ M-2\rangle|^2 = (I-M+2)(I+M-1)(I-M+1)(I+M) \quad (a)$$

$$|\langle M|\ I_-^2|\ M+2\rangle|^2 = (I+M+2)(I+M+1)(I-M)(I-M-1) \quad (b)$$

$$|\langle M|I_zI_+ + I_+I_z|M-1\rangle|^2 = 4M^2(I-M+1)(I+M) - 4M(I-M+1)(I+M)4(I-M+1)(I+M) \quad (c)$$

$$|\langle M|I_zI_- + I_-I_z|M+1\rangle|^2 = 4M^2(I+M+1)(I-M) + 4M(I+M+1)(I-M)+(I+M+1)(I+M). \quad (d)$$

(7) Line Shape Information

Abragam (18) defines the $\underline{\underline{K}}$ -matrix in terms of an $\underline{\underline{A}}$-matrix thus allowing one to assemble information about line shape, i.e

$$I(\omega) \propto - \mathrm{Re}\{\vec{\omega} \cdot \underline{\underline{A}}^{-1} \cdot \vec{1}\} \text{ for the S-spectrum} \quad (21)$$

where $\vec{\omega}$ is a row vector whose components are proportional to the relative population of the spin states of the I-nucleus -- neglecting the Boltzmann factor (high temperature approximation), and where $\vec{1}$ is a unit column vector. $\underline{\underline{A}}^{-1}$ is the inverse of the $\underline{\underline{A}}$-matrix given by

$$\underline{\underline{A}} = i\,\underline{\underline{\omega}} + \underline{\underline{K}} + \underline{\underline{R}}_2 \quad (22)$$

where $\underline{\underline{\omega}}$ is the diagonal matrix of the discrete site precession frequencies, the kinetic relaxation matrix, $\underline{\underline{K}}$, describes the transfer of magnetization of the nuclear magnetic energy level spectrum between sites and the relaxation matrix $\underline{\underline{R}}_2$ is the diagonal matrix of the transverse relaxation rate associated with other relaxation mechanisms excluding the $\underline{\underline{K}}$ processes.

Hence knowledge of the transition probability per

unit time of transitions occurring between states M and M′ of spin 1 as stated in the relaxation mechanisms mentioned in sections 2, 3, 4, 5, 6 of this chapter allow a calculation of the $\underline{\underline{K}}$-matrix to be performed and subsequently total analysis of the spectral line shape.(26)

CHAPTER III

EXPERIMENTAL AND RESULTS

non sine pulvare palma

(1) Experimental

(a) Material Used and Sample Preparation

WF_6 and MoF_6 (Alfa Inorganics) were purified according to the procedure of T. A. O'Donnell (27) by placing approximately 3 gms of reagent grade NaF into the apparatus (see Fig. 1). A cylinder of MoF_6 (or WF_6) was attached to the vacuum system which was then evacuated and baked out for a day, the whole vacuum system having been carefully checked for leaks. An acetone-dry-ice bath was placed under trap 1 and a liquid N_2 bath under trap 2. The tap of the cylinder containing the hexafluoride was opened for about three minutes and the hexafluoride was thus admitted and trapped in trap 1. Stop-cock 1 was then closed and the liquid N_2 bath and subsequently the dry-ice-acetone bath, removed. The whole system was warmed to room temperature and the hexafluoride allowed to remain over the NaF for about an hour, causing removal of any HF. The hexafluoride was then frozen again, using two liquid N_2 baths, at traps 1 and 2 respectively. The cylinder containing the hexafluoride was subsequently sealed from the vacuum system and removed. Stop-cock 1 was opened and the system pumped on for about an

half-hour, at the end of this period the apparatus was sealed in front of trap 2 and removed from the cold baths and vacuum system. This freeze-thaw-freeze-pump procedure was performed to alleviate any pressure build up within the apparatus, by contact of the hexafluoride and the impurities in the glass. The system was allowed to stay at room temperature for a day, at the end of which time the apparatus shown in Fig. 1 was joined to the apparatus shown in Fig. 2 and the purification process described in the above procedure was carried one stage further. Once again, the procedure was performed under vacuum in a dry leak-proof system. The hexafluoride was removed from trap 1 and passed into trap 3, which also contained reagent grade NaF, by subjecting a temperature differential across the two traps. When all the hexafluoride had been transferred to trap 3, that part of the apparatus containing trap 1 was sealed off and removed. The freeze-thaw-freeze-pump procedure mentioned above was repeated once more; this time the hexafluoride remained at room temperature for only four hours, before a sample was transferred to one of the two N.M.R. tubes by conventional methods, the second transfer being carried out a day later. In both cases it was the second sample that was used to give the F^{19} spectra, as it was suspected that these samples might be of higher purity. The purity, of these samples, was checked by scanning the complete range, i.e., 46.5 Khz to 65.5 Khz, of the F^{19} spectra using a Varian Associates A56/60 N.M.R. spectrometer at 56.4 Mhz.

For MoF_6, absorption peaks were noted only after attaching to the N.M.R. spectrometer a Schomandl ND30M external frequency synthesiser set at 72.5 Khz; while WF_6 gave absorption peaks only when the frequency offset was set at +8 Khz, or the external frequency synthesiser set at the equivalent 65.5 Khz.

Figure 3 shows the F^{19} spectrum of MoF_6 (30). It consists of a weak sextet associated with the I = 5/2 molybdenum isotopes, and a strong singlet attributed to the I = 0 molybdenum isotopes, table 1. Due to the ratio $\mu^{95}/\mu^{97} = 1.02$ the sextet was separated into sharp components, attributed to Mo^{95}, and much broader components, attributed to Mo^{97}, by visual inspection.

To determine whether it was correct to make the above assumptions, the two components of any one peak were cut from the spectrum and weighed. The ratios of the weights ($Mo^{95}F_6/Mo^{97}F_6 = 1.73 \pm 0.12$ gms) were found to be, within experimental error, the ratios of the percent abundance ($Mo^{95}/Mo^{97} = 1.64$ Table 1), confirming the assumption made.

Figure 4 shows the F^{19} spectrum of WF_6, consisting of a medium intense doublet, attributed to W^{183} I = $\frac{1}{2}$, and a very intense singlet attributed to the I = 0 isotopes of tungsten (Table 1).

Analysis of the high resolution N.M.R. F^{19} spectra over a range of temperatures gave the temperature dependence of the metal spin relaxation processes. This was done by

measuring the respective widths at half-height for Mo^{97}. For Mo^{95} the temperature dependence of the width at half-height of each peak was obtained by measuring the width at half-height of the broadest peak, and the peak height of each peak from the 'new' base-line. The peak height was obtained accurately by considering the Boltzmann Distribution Law, with reference to 42°C as a standard. In WF_6 the temperature dependence of the widths at half-height was obtained by measuring the width at half-height of both peaks and taking the average of these values. The temperature ranges investigated were:

(a) MoF_6 22°C to 68°C

(b) WF_6 9.5°C to 59.5°C

To maintain a high degree of reproducibility in doing these temperature runs, the spectrometer was first checked for homogeneity by observing the proton spectrum of H_2O at 60 Mhz for each temperature. The temperature of the particular run was observed by measuring the frequency separation for the two peaks of the proton spectrum of ethylene glycol or methanol and referring to plots in Fig. 5 or 6. The spectrometer was then switched to 56.4 Mhz to observe the F^{19} spectrum of the hexafluoride, the homogeneity of the instrument being maximised again by locating one of the peaks of the sextet, or 'sitting on' one of the peaks of the doublet and repeating the maximising process for each peak recorded.

To maintain reproducibility in the spectra of MoF_6, the filter bandwidth was maintained at 4 hz and the r.f field at 0.03 mgauss, while the sweep rate was maintained at 0.1 hz sec^{-1} and the spectral amplitude at 50. For WF_6 the filter bandwidth was maintained at 4 hz and the r.f field at 0.02 mgauss while the sweep rate was maintained at 0.1 hz sec^{-1}, the spectral amplitude being 5.0.

The separation J_{Mo}-F and J_{W-F} between adjacent peaks of the respective spectra was obtained by placing side-bands on the two outer peaks of the sextet and doublet, respectively, from the intense centre band, using a Hewlett-Packard 3300 A function generator connected to a C.M.C. Model 201 B frequency period counter which was connected to the spectrometer. This gave

$$J_{Mo^{95}-F} = 46.7 \pm 0.1 \text{ hz}$$

$$J_{W^{183}-F} = 43.8 \pm 0.1 \text{ hz}$$

(ii) Results

Table 1 consists of a list of the nuclear properties (with references) of W and Mo.

(a) Molybdenum Hexafluoride:

To verify the results of the F^{19} T_1 experiments on MoF_6 performed by Rigny and Virlet (24), a Π - $\Pi/2$ T_1 pulse experiment was performed at 60 Mhz and 29°C (Fig. 7). The results obtained were plotted in Fig. 8 (R_{IF} = 1.2 sec^{-1})

and found to be in agreement with Rigny and Virlet's (24) data, within experimental error.

Table 2 contains the peak widths at half-height for $Mo^{97}F_6$, as a function of temperature, with the corresponding values of $R_{1Q}97$ obtained using Equation 18 Chapter II, as pointed out in Chapter IV. The diagonal values of this $\underline{\underline{K}}$-Matrix(15 : 23 : 18) are associated with the average peak-widths at half-height of the two corresponding peaks of the sextet. Using these coefficients it was possible to obtain a value for the quadrupolar term α, provided a true lorentzian line shape is obeyed, and other line broadening mechanisms are negligible. The derived relaxation plot for Mo^{97} was found to be linear (Fig. 9 plot labelled $R_{1Q}97$).

The multiplets due to Mo^{95} were treated similarly. Knowing the ratio $(eQ^{95}/eQ^{97})^2$ (28)(29) and $R_{1Q}97 = 1/T_{1Q}97$ at each temperature, it was possible to calculate $R_{1Q}95$ since

$$R_{1Q}95 = (eQ^{95}/eQ^{97})^2 \; R_{1Q}97 \; , \qquad (1)$$

values for $R_{1Q}95$ are collected in table 3.

Knowing the R_{1F} data from Rigny and Virlet's pulse experiments on MoF_6 (Fig. 9 plot labelled $R_{1F\ (R+V)}$), and the peak widths at half-height (corrected), it was possible to utilise the transition probability for the spin-rotation interaction (Equation 13 Chapter II) with the associated $\underline{\underline{K}}$-Matrix diagonal elements (Appendix 2 Equation 1) i.e.,

5 : 13 : 17, to calculate the F^{19} linewidth contribution for Mo^{95} spin-rotational interaction (the spin-rotation interaction term) i.e.

$$\Delta\nu_{observed} = \Delta\nu_{R_{1F(R+V)}} + \Delta\nu_{R_{1Q^{95}}} + \Delta\nu_{R_{1Mo^{95}}} + \Delta\nu_{R_2}^{*} \qquad (ii)$$

where R_2^* is a measure of the field in-homogeneity. Assuming Lorentzian behaviour, equation (ii) only applies if these are the only contributing mechanisms. Chapter IV will give reasons for discarding all other mechanisms mentioned in Chapter II. That we were justified in assuming lorentzian behaviour may be obtained by referring to the plot, Fig. 9, obtained from table 4 for $R^*_{Mo^{95}}$.

(b) Tungsten Hexafluoride

Mo and W appear in the same group of the periodic table, and because of the 'lanthanide contraction', associated with a full 4f orbital, they have approximately the same atomic radii; it might be suspected that the electronic interactions with these two nuclei are similar.

As the dominant relaxation mechanism in Mo^{95} is spin-rotation interaction and since tungsten has a spin, $I = \frac{1}{2}$, nucleus, it might be expected that the dominant relaxation mechanism for W^{183} is also spin-rotation interaction. To obtain information on line broadening due to the W^{183} centre three methods were attempted, since this particular contribution was very small.

Firstly, the full-width at half-height of the proton spectrum of TMS in $CDCL_3$ should give a measure of the magnet inhomogeneity. This value may be subtracted from the F^{19} spectrum of the W^{183} doublet, from which R_{1_F} had already been subtracted. However, due to impurity, the line width was wider than expected and this technique was discarded.

Secondly, the Rotary Echo experiment was attempted at 56.4 Mhz sitting on one of the peaks of the W^{183} doublet. Magnetic inhomogeneity effects were refocussed by this technique, and therefore contributed nothing to the end result. However, the separation from the intense W ($I = 0$) peak to the weak W^{183} ($I = \frac{1}{2}$) peaks was ≈ 21.6 hz., and as a result, the overlap of this intense peak with the weaker peaks nullified the usefulness of this experiment and no results were obtained.

Thirdly, Pople et al (Chapter 3 of (31)) point out that if the rate of change of H_0 is fast enough, the signal changes its shape and shows a series of characteristic wiggles (Fig. 10) in the tail after passing resonance. The decay of this 'envelope' is of the order of the transverse relaxation time, T_2. However, during this period the magnetic moment vector $\vec{M}$ and the r.f. field H_1 will be rotating about the direction of H_0 at different rates, so that they will alternately go in and out of phase. The absorption signal which measures the out of phase component will show a series of damped oscillations through resonance. Performing this experiment on each of the

peaks of tungsten doublet, and recording the decay signal on a recording scope will yield a value for $(R_2)_{\text{wiggle beat}}$ where:

$$(R_2)_{\text{wiggle beat}}^{\text{observed}} = R_{2_F} + R_2^* + R_{\text{radiation damping}} + R_{1_W} \qquad \text{(iii)}$$

To remove the effects of radiation damping, which Abragam (P_{76} (18)) points out is a function of the magnetization M_0, the filling factor η and the Q of the tuned receiver circuit.

$$2H_r = 4\pi\eta Q M_0 \sin\theta \qquad \text{(iv)}$$

which in turn yields a characteristic time τ given by

$$\tau = (2\pi Q \chi_0 \omega_0)^{-1} \qquad \text{(v)}$$

where ω_0 is the larmor frequency and where τ is found to be shorter than T_2 due to suppression of the free precession of the nucleus. Detuning the spectrometer off-resonance decreases the radiation damping by the factor Q'/Q. Performing this experiment on the intense centre line $(R_2)_{\text{wiggle beat}}$ may be defined as:

$$(R_2)_{\text{wiggle beat}} = R_{1_F} + R_2^* \qquad \text{(vi)}$$

since for the centre peak W (I = 0).

Assuming the effects due to radiation damping are small, a value for $R_{1_W 183}$ may be obtained by subtracting (vi) from (iii). This experiment did not work because the line-widths do have a factor associated with inhomogeneity.

However, by combining the fast sweep method for the centre peak, the instrument having been detuned, with the conventional F^{19} High Resolution N.M.R. experiment on WF_6 a value for R_{1_W} was obtained. This experiment was performed at a series of temperatures and an analysis of the results made using Equation 13, Chapter II with the associated $\underline{\underline{K}}$-Matrix diagonal elements (Appendix II, $I = \frac{1}{2}$). These results are collected in table 5 and only apply if this is the dominant nuclear spin relaxation mechanism, and if the 'slow W^{183} relaxation limit' holds, so that the lines are lorentzian. This data is plotted in Fig.11 labelled $R_{1_W 183}$ from which the small relaxation effect due to W^{183} is noted, as well as the trend of increasing R with decreasing temperature, associated with a spin rotational interaction.

CHAPTER IV

DISCUSSION

Festina Lente

(1) General

In this chapter an attempt will be made to show why the spin-rotation and quadrupolar nuclear spin relaxation mechanisms are the dominant relaxation mechanisms of the central metal nuclei of molybdenum and tungsten hexafluorides. Comparison of the results obtained by F^{19} N.M.R., with those from the diffusion experiments of Rigny and Virlet (24) for MoF_6 and WF_6, suggested a means of comparing the activation energies associated with molecular rotation, as obtained by N.M.R., with those obtained by the classical diffusion coefficient as suggested in Debye's 'Polar Molecules' Chapter 5 (32). This comparison has lead to a critical study of the different correlation times.

(2) Dominant Relaxation Mechanisms at the Mo Nuclei in MoF_6

It was possible to eliminate nuclear spin relaxation by an intra-molecular dipole-dipole mechanism by utilising the theory on this mechanism outlined in section 2 Chapter II. Using the transition probability out of any site for the F^{19} nucleus (Equation 6 Chapter II) Rigny and Virlet (24) eliminated an intramolecular dipole-dipole relaxation mechanism i.e.

$$P_{MM}(F) \propto 4 \gamma_F^4 / r_{F-F}^6 \qquad (a)$$

Considering an intramolecular dipole-dipole mechanism at the Mo nucleus (Equation 6 Chapter II) allow a calculation of the transition probability out of any site for the Mo nucleus i.e.

$$P_{MM'}(Mo) \propto 6 \gamma_F^2 \gamma_{Mo}^2 / r_{Mo-F}^6 \qquad (b)$$

making use of Rigny and Virlet's result, and comparing the ratio

$$\frac{P_{MM'}(Mo)}{P_{MM'}(F)} \propto \frac{6\gamma_{Mo}^2}{4\gamma_F^2} \frac{r_{F-F}^6}{r_{Mo-F}^6} = 5.46 \times 10^{-2}$$

allows us to discard this mechanism. Further evidence for not considering this mechanism came from the temperature dependence plots (Fig. 9). Mo^{95} was shown to give the opposite temperature dependence to what would be expected for an intramolecular dipole-dipole mechanism. Although Mo^{97} gave the same type of slope, as would be expected for a dipole-dipole mechanism, this was only to be expected, since a quadrupole mechanism was used to obtain this plot, and both quadrupole and dipole-dipole relaxation mechanisms depend in similar manner on the molecular orientation, with respect to the laboratory reference frame.

Since the <u>intermolecular</u> dipole-dipole relaxation mechanism uses the distance of closest approach, a, between

the I-spin considered and a neighbouring S-spin (Chapter II, Section 3), and because of the similarity of the expressions for the transition probability (Equations (6) and (7) Chapter II), it becomes possible to eleiminate this mechanism, in like manner as the intramolecular dipole-dipole mechanism.

The transition probabilities associated with chemical shift anisotropy, as set out in Equation 9 Chapter II are proportional to $\gamma_{Mo}^2 \cdot H_0^2 \cdot \overline{\nabla}_z^2$ and since we were obtaining information about the central metal nucleus, which was in a spherical environment, $\overline{\nabla}_z = 0$ and the mechanism is ineffective to first order.

These eliminations leave nuclear spin relaxation mechanisms associated with spin-rotation and quadrupolar interactions at the Mo nuclei in MoF_6, and the possibility of higher order nuclear interactions.

In considering the two field gradient mechanisms mentioned in Section 6 Chapter II an estimation of the nuclear centrifugal distortion was made using the values $\overline{\omega}_e = 741$ cm^{-1} for the totally symmetric stretching frequency ν_1, (33), $r_{ij} = 1.9$ Å (24) in Equation 15 Chapter II. A maximum J = 50 was used in this calculation, since this was the value expected at temperatures of about 70° C, assuming equipartition of energy. The result of performing this calculation indicated that such a distortion yields a bond extention r_j / r_e of about 4×10^{-4} perpendicular to the rotation axis, and hence could not account for any sizable molecular field gradient for quadrupolar

coupling.

Another means through which a quadrupolar mechanism might operate in a spherical environment entails disrupting the molecular symmetry via intermolecular collisions, as pointed out in Chapter II, Section 6 (b). Using the transition probabilities associated with this mechanism (Equation 18 Chapter II) the corresponding $\underline{\underline{K}}$ - Matrix for $I = 5/2$ was obtained (Appendix II). The ratio of the transition probabilities to the square of the matrix elements yields a value for the spin-lattice relaxation rate R_{1_I} It was found that quadrupolar relaxation was the dominant mechanism of Mo^{97} (Fig. 9 plot labelled $R_{Mo}97$) due to its large nuclear quadrupole moment (Table 1). The slope of this plot yielded an activation energy of (1.4 ± 0.2) Kcals mole $^{-1}$.

The dominant relaxation mechanism observed for Mo^{95} was spin-rotation, as pointed out in Chapter III. A temperature dependence plot for this mechanism (Fig. 9 plot labelled $R_{I \cdot J}$ Mo^{95}) yielded an activation energy of (2.2 ± 0.3) Kcals mole $^{-1}$. Since these relaxation mechanisms completely accounted for the observed F^{19} multiplet line widths we conclude that higher multipole relaxation mechanisms (e.g., electric hexadecapole) are absent. Since the F^{19} T_1 pulse experiment agrees with Rigny and Virlet's results, within experimental error, it was possible to conclude that there were no paramagnetic species present in the solution of MoF_6. As the

activation energies for quadrupolar and spin-rotation interactions of the Mo nuclei were found to be an order of magnitude lower than the energy required to break the Mo-F bond, it was concluded that no chemical exchange phenomena occurred in this sample.

(3) Dominant Relaxation Mechanisms at the W^{183} Nucleus of WF_6

Due to the similarity in the bond lengths r_{W-F} and r_{Mo-F}, caused by the 'lanthanide contraction', and since for MoF_6 inter- and intra- molecular dipole-dipole mechanisms were discarded, in like manner inter- and intra- molecular dipole-dipole relaxation mechanisms may be discarded for WF_6. As with the Mo nuclei, it was also possible to eliminate relaxation due to chemical shift anisotropy, because of the spherical symmetry at the W^{183} centre. Also W^{183} has spin $I = \frac{1}{2}$ and consequently no quadrupole or higher moment.

A dominant spin-rotational relaxation mechanism was thus expected for W^{183}. This mechanism was supported by the observed temperature dependence (Fig. 11 plot labelled $R_{1_{W183}}$). The approximate activation energy measured from the slope of this plot is (3.4 $\pm$ 1.1) Kcals $mole^{-1}$.

Since this mechanism accounts for the observed F^{19} line widths; it was possible to discount any extra broadening process due to paramagnetic impurities, chemical exchange, etc. Chemical exchange is also ruled out from the magnitude of the observed activation energy.

(4) Correlations between Spectroscopic and Diffusion Results

The values of the activation energies associated with the spin-rotation relaxation mechanisms associated with Mo^{95} and W^{183} and the quadrupolar relaxation mechanism of Mo^{97} were compared with the results of the diffusion experiments on MoF_6 and WF_6 obtained by Rigny and Virlet (24). The disagreement between these values points out the weakness in correlating nuclear spectroscopic results on relaxation concerning molecular rotations with the classical model of Brownian translational diffusion.

To analyse this model for relaxation the approach taken by Debye (32) will be used in defining the relaxation time and the correlation function i.e., by considering his description of the anomalous dispersion and absorption of polar liquids. This model assumes that it is possible to relate information obtained from translational diffusion to rotational diffusion by relating the correlation times for these two processes i.e., $\tau = 9\tau_0$ Debye states 'that for a rotating sphere of radius, a, the relaxation time should be represented by

$$\tau_0 = 4\pi\eta a^3/3kT \qquad (1)$$

where η is the inner friction constant, as defined by Stokes' This relation, however, was derived by Debye for the theory of dielectric relaxation of polar liquids, and does

not strictly apply to our spherical molecule. In correlating diffusion, τ_θ may be related through a diffusion equation to a rotational diffusion constant D_r, and hence to the microscopic viscosity, η, and the molecular diameter, a, through the Stokes-Einstein relation (32)

$$D_r = kT/\pi a^3\eta \qquad (2)$$

Hence in analyzing molecular motions on the basis of the above considerations, one presupposes a specific model for the type of random motion. Another model often used assumes that reorientation is a thermally activated process, by which the molecule as a whole flips from a torsionally oscillating state in one potential minimum to a similar state in an equivalent minimum (34). This model leads to the relation

$$\tau_\theta = \tau_\theta^0 \, e^{+E/kT} \qquad (3)$$

where E is the activation energy related to the height of the potential barrier separating the minima. When as commonly occurs $1/T_1$ depends on temperature in a manner consistant with the preceeding equation, one is, to a degree, justified in accepting the model proposed and proceeding to draw conclusions about the activation energy.

To account for the quadrupolar interaction in the case of a spherical molecule having a nuclear quadrupole moment ($Mo^{97}F_6$), an intermolecular stimulated relaxation mechanism

has been suggested. The model used in this case suggests that intermolecular collisions are responsible for distorting the molecular electron cloud causing a field gradient to arise. To suggest that this model has a correlation time τ, which is a function of a second order spherical harmonic, may be seen by realising that instantaneous distortions to the molecular symmetry caused by collisions allow a measure of the reorientation, occuring exponentially in time, of the disturbed spin system at thermal equilibrium. This is similar to the relaxation mechanism of Xe^{131} observed by Staub (41), in which distortion of the atom occurs chiefly by the Van der Waals forces, allowing for the establishment of an efficient quadrupolar relaxation mechanism ($I_{xe} = 3/2$). However, Staub mentinns that the correlation time, , differs from that defined by Bloembergen, Purcell and Pound (7), because of the statistical time dependence of the field gradient caused by collisions with a uniform spectrum of frequencies to frequencies of the order $\omega \simeq 1/\tau \gg \omega_o$. Staub then says that $Ro/\tau = Ro/\bar{v}$. Hence

$$1/T_1 \simeq 1/T_2 = \frac{3\pi}{80} \frac{NR_o^4}{\bar{v}} \left(\frac{eqQ}{\hbar}\right)^2 \left(\frac{C_w/R_o^6}{E_1 - E_o}\right) \frac{I^2 + I - 3/4}{I^2(2I - 1)^2} \quad (a)$$

Where R_o is the minimum distance between two molecules, C_w is defined in terms of the Van der Waals constants α and β, and $\bar{v}$ is the average speed of the molecule, while $E_1 - E_0$ is the energy for a transition.

It should be kept in mind that these distortions are only instantaneous and are, in fact, time averaged to zero.

The usual model of a spin-rotational interaction which has been shown by Hubbard (14) to be a function of the angular momentum of the molecule, since the nucleus jumps from one J - state to another, may be considered for $Mo^{95}F_6$ and WF_6. In this case no viscosity term should appear in the Stoke's-Einstein model (Equation 2).

Several papers have recently appeared in the literature attempting to correlate microscopic results to N.M.R. (35), (36), (37), (38). All of these papers consider the Brownian motion of colloidal particles floating in a liquid medium and all suggest that any fluctuations occurring are due to this type of motion. However, the attack on this problem changes with the model used (e.g., hard core or soft core, etc.). The general approach taken by chemists in the theory of transport phenomena tends to emphasize a model based on the kinetic theory of gases.

(4) Relation between τ_θ and τ_q

By considering the theory of translational Brownian motion of a spherical particle and using the Langevin equation

$$du/dt = - BU + A(t) \qquad (4)$$

where U denotes the linear velocity of the particle, Hubbard (14) obtains expressions for the conditional probability density for the velocity of the molecule. Modifying (4) to consider rotational Brownian motion Hubbard obtains an expression for

the probability density for the angular velocity of a spherical particle. From a knowledge of the angular momentum of a spherical molecule, and considering the latter of the two conditional probabilities he defines

$$\tau_q \equiv \tau_1 = 1/B' \tag{5}$$

where

$$f' \equiv I B' \tag{6}$$

where f' is the friction constant and I is the moment of inertia of the molecule.

Hubbard then uses the diffusion coefficient D' occurring in Furry's theory, relating it to the viscous retarding torque per unit angular velocity i.e., Equation(6) by

$$D' = k T/f' \tag{7}$$

and by the use of Wigner rotation matrices he defines

$$\tau_\theta = (6D')^{-1} \tag{8}$$

from which it follows that

$$\tau_q \tau_\theta = (I/6kT) \tag{9}$$

However the theory used by Hubbard is only valid when heavy particles are immersed in a light medium and may not be valid for identical interacting molecules.

Rigny and Virlet (24) point out that still more difficulties arise, since it is not obvious, particularly for spherical molecules, why the diffusion equation should be obeyed, and the parameters governing rotational motions cannot be simply deduced from the corresponding parameters of translational motion. This suggests the inadequacy of the usual techniques mentioned in Section (4) to our problem. By gleaning information on both transport properties and rotational Brownian motion from Mori's paper (39), and by utilising the Fluctuation-Dissipation Theorem of Kubo (40), Rigny and Virlet were able to obtain information which did not require that the particle under observation be heavier than the molecules interacting with it. However, to re-calculate a new relationship between τ_θ and τ_c is beyond the scope of this thesis.

(6) Further Work?

Since the order of magnitudes of the line widths being measured were less than 1 hz for the spin-rotation interaction, the N.M.R. spectrometer was being pushed to its limits. The results may be improved by connecting to the machine a signal averager; with this instrument the results could be recorded in digital code which could be analysed by computer!

A theory on transport properties should be developed to consider the relations between the correlation times used i.e., τ_θ and τ_c ; however, it would be advisable for such a

theory to take an approach which differs from the Debye theory, because of the spherical symmetry and uncharged nature of the system.

BIBLIOGRAPHY

1. W. Gordy, Discussions of the Faraday Soc. 19, 14 (1955).
2. W. J. Moore, 'Physical Chemistry' Chap. 11 (3rd Edition, Prentice-Hall, 1963).
3. N. Bloembergen, Thesis Leiden 1948.
4. W. Pauli, Naturwissenschaften 12, 741 (1924).
5. H. Schuler, T. Schmidt, Z Phys. 94, 457 (1935).
6. R. V. Pound, Phys. Rev. 79, 685 (1950).
7. N. Bloembergen, E. Purcell, R. Pound, Phys. Rev. 73, 679 (1948).
8. H. Dehmelt, H. Kruger, Naturwissenchaften 37, 111 (1950); 38, 921 (1951).
9 T. Wang, Phys. Rev. 99, 566 (1955).
10. R. J. Mahler, T. James, Phys. Rev. Letters 16, 259 (1966).
11. R. J. Mahler, W. James, Proc. XIVth Colloq. A.M.P.E.R.E. 14, 938 (1967).
12. H. P. Mahon, Proc. XIVth Colloq. A.M.P.E.R.E. 14, 936 (1967).
13. I. V. Aleksandrov, 'Theory of Nuclear Magnetic Resonance' Chap. 1 (Academic Press 1966).
14. P. S. Hubbard, Phys. Rev. 131, 1155 (1963).
15. P. W. Atkins, Molecular Physics 12, 133 (1967).
16. M. Bloom, Can. J. Phys. 43, 486 (1965).
17. R. J. Brown, H. S. Gutowsky, H. Shimomura, J. Chem. Phys. 38, 76 (1963).
18. A. Abragam, 'Principles of Nuclear Magnetism' (Oxford University Press 1961).
19. R. Lynden-Bell, 'Progress in N.M.R. Spectroscopy' Vol. 2 J. Emsley, J. Feeney, L. Sutcliffe (Pergamon Press 1967).

20. C. Slichter, 'Principles of Magnetic Resonance' (Harper Row 1963).

21. J. Waugh, Proc. XIVth Colloq. A.M.P.E.R.E. 14, 113 (1967).

22. H. Gutowsky et al. Phys. Rev. Letters 6, 349 (1961).

23. W. Moniz, H. Gutowsky, J. Chem. Phys. 38, 1155 (1965).

24. P. Rigny, J. Virlet, J. Chem. Phys. 47, 4645 (1967).

25. C. Banwell, 'Fundamentals of Molecular Spectroscopy' p. 42 (McGraw-Hill 1966).

26. H. Gutowsky, R. Vold, E. J. Wells, J. Chem. Phys. 43, 4107 (1965).

27. T. A. O'Donnell, J. Chem. Soc. 4681 (1956).

28. A. Narath, D. Alderman, Phys. Rev. 143, 328 (1966).

29. A. Kaufman, Z Physik 182, 217 (1964).

30. P. Rigny, A. Demortier, Compt. Rend. 263B, 1408 (1966).

31. J. Pople, W. Schneider, H. Bernstein. 'High Resolution Nuclear Magnetic Resonance' (McGraw-Hill 1959).

32. P. W. Debye, 'Polar Molecules' (Chemical Catalog Co. 1929).

33. G. Herzberg, 'Electronic Spectra of Polyatomic Molecules' (Van Nostrand 1966).

34. J. Waugh, 'Molecular Relaxation Processes' (Academic Press 1966).

35. M. Bloom, Proc. XIVth Colloq. A.M.P.E.R.E. 14, 63 (1967).

36. W. Steele, J. Chem. Phys. 38, 2404 (1963).

37. R. McClung, D. Kivelson, J. Chem. Phys. 49 3380 (1968).

38. K. Wirtz, A. Spernol, Z Naturforsch. 8a 522 (1953).

39. H. Mori, Progress In Theoretical Physics (Japan) 33, 423 (1965).

40. R. Kubo, Report on Progress in Physics 29, 255 (1966).

41. H. Staub 29 246 (1966)

APPENDIX I

The total Hamiltonian for a general relaxation process may be written in terms of a perturbation Hamiltonian $\hbar\mathcal{H}(t)$ where

$$\mathcal{H}(t) = \sum_q F^{(q)}(t) \quad A^{(q)} \tag{1}$$

where $F^{(q)}(t)$ is a random lattice function of time and $A^{(q)}$ a random operator acting on the spin variables. (18) Following Abragam (18) an expression for the transition probability of spin I may be obtained as

$$P_{MM'} = |\langle M | A | M \rangle|^2 \mathcal{J}(\omega_{MM'}) \tag{2}$$

where $\mathcal{J}(\omega_{MM'})$ is the spectral density at the transition frequency $\omega_{MM'}$ which can be written in terms of an auto-correlation function as follows:

$$\mathcal{J}(\omega) = \int_{-\infty}^{\infty} g(\tau) \quad e^{-i\omega\tau} d\tau \tag{3}$$

where

$$g(\tau) = \overline{F^{(q)}(t) \quad F^{(q)}(t+\tau)} \tag{4}$$

If it is assumed that the fluctuations of $\mathcal{H}(t)$ are such that the auto correlation function $g(\tau)$ decays exponentially the integration may be carried out. It has been found that this type of autocorrelation function follows from the assumptions made in the theory of Brownian motion and leads to a lorentzian line shape. Hence it

is possible to write

$$g(\tau) = e^{-\tau/\tau_c} \qquad (5)$$

where τ_c is the correlation time characteristic of the fluctuations of $\mathcal{H}(t)$. Substituting (5) in (2) we obtain

$$P_{M,M'} = |\langle M|A|M'\rangle|^2 \frac{2\tau_c}{1+\omega^2\tau_c^2} \qquad (6)$$

$$= |\langle M|A|M'\rangle|^2 2\tau_c \qquad (7)$$

in the extreme narrowing limit i.e. $\omega^2\tau_c^2 \ll 1$.

To evaluate the $\langle M|A|M'\rangle$ Matrix elements use is made of the relations:

$$\langle M|I_{\pm}|M \mp 1\rangle = [(I \pm M)(I \mp M + 1)] \qquad (8)$$

APPENDIX II

The transition matrix of $\underset{\sim}{K}$ - matrix (chapter II Equation 22) can be evaluated from the respective transition probability of the associated nuclear spin relaxation mechanism.

For $I = 5/2$ the $\underset{\sim}{K}$ - matrix of the associated spin-rotation interaction becomes:

$$\underset{\sim}{K}_I \cdot J = \begin{array}{c} M_I \\ \\ 5/2 \\ 3/2 \\ 1/2 \\ -1/2 \\ -3/2 \\ -5/2 \end{array} \begin{array}{c} \begin{array}{cccccc} 5/2 & 3/2 & 1/2 & -1/2 & -3/2 & -5/2 \end{array} \\ \begin{bmatrix} -5 & 5 & 0 & 0 & 0 & 0 \\ 5 & -13 & 8 & 0 & 0 & 0 \\ 0 & 8 & -17 & 9 & 0 & 0 \\ 0 & 0 & 9 & -17 & 8 & 0 \\ 0 & 0 & 0 & 8 & -13 & 5 \\ 0 & 0 & 0 & 0 & 5 & -5 \end{bmatrix} \end{array} \frac{C^2 IkT\tau_s}{\hbar^2}$$

For I = 1/2 the K - Matrix associated with the spin-rotation interaction becomes:

$$\underset{\sim}{K}_{I\cdot J} = \begin{array}{c} M_I \backslash M_I \\ 1/2 \\ -1/2 \end{array} \begin{array}{c} \begin{array}{cc} 1/2 & \quad -1/2 \end{array} \\ \begin{bmatrix} -1 & 1 \\ 1 & -1 \end{bmatrix} \end{array} \times \frac{C^2 I k T \tau_c}{\hbar^2}$$

For I = 5/2 the K-Matrix associated with nuclear electric quadrupolar relaxation may be obtained in terms of R_1 by modifying Equation 18 of Chapter II to give

$$P_{M_I M\pm 2} = \frac{R_1}{2(2I+3)(2I-1)} \left| \langle M \mid I_{\mp}^2 \mid M\pm 2 \rangle \right|^2$$

$$P_{M_I M\pm 1} = \frac{R_1}{2(2I+3)(2I)} \left| \langle M \mid I_{\mp} I_z + I_z I_{\mp} \mid M\pm 1 \rangle \right|^2$$

from which

$$K_Q = \begin{array}{c} M_I \backslash M_I I \\ 5/2 \\ 3/2 \\ 1/2 \\ -1/2 \\ -3/2 \\ -5/2 \end{array} \begin{array}{c} \begin{array}{cccccc} 5/2 & 3/2 & 1/2 & -1/2 & -3/2 & -5/2 \end{array} \\ \begin{bmatrix} -15 & 10 & 5 & 0 & 0 & 0 \\ 10 & -23 & 4 & 9 & 0 & 0 \\ 5 & 4 & -18 & 0 & 9 & 0 \\ 0 & 9 & 0 & -18 & 4 & 5 \\ 0 & 0 & 9 & 4 & -23 & 10 \\ 0 & 0 & 0 & 5 & 10 & -15 \end{bmatrix} \end{array} \times \frac{R_1}{8}$$

GLOSSARY OF TERMS

SYMBOL	MEANING
I	Nuclear spin quantum number.
$\hbar$	Planck's constant on 2π .
γ	Nuclear magneto-gyric ratio.
H_0	Applied magnetic field.
k	Boltzmann constant.
T	Temperature ^{0} Kelvin.
M_0	Curie magnetization.
M_Z, M_X, M_Y	Magnetization along a cartesian axis.
$1/T_1=R_1$	Spin lattice relaxation rate constant.
$1/T_2=R_2$	Longitudinal relaxation rate constant.
τ_c, τ_θ	Correlation times
$F^{(q)}(t)$	Lattice operators
$P_{MM}1$	Transition probability out of a Zeeman state M .
$H^1(t)$	Time dependent Hamiltonian.
$\underline{\underline{\sigma}}$	Chemical shift shielding tensor.
$\underline{\underline{C}}$	Spin-rotational interaction constant.
$J(t)$	Molecular angular momentum.
$g(\omega)$.	Autocorrelation function.
$\mathcal{J}(\omega)$	Spectral density at angular frequency .
c	Speed of light.
B	Molecular nuclear rotational constant.
I_B	Moment of inertia.
D	Molecular nuclear centrifugal distortion constant.

eq	Molecular electrostatic field gradient.
$\Delta\nu$	Full line width in hz.
eQ	Nuclear quadripole moment.
η	Inner friction constant.
	Rotational diffusion constant.
α	Quadrupolar relaxation coefficient.
β	Spin-rotation interaction coefficient.
R_2^*	Transverse dephasing rate due to magnet inhomogeneity.

TABLE 1

NUCLEAR PROPERTIES OF F, Mo, W.

Isotope	N.M.R. frequency in Mhz for a 10 mgauss field	Natural abundance %	Magnetic Moment (μ (N.M.))	Spin I in multiples of $\hbar$	Electric Quadrupole Moment Q($\times 10^{-24} cm^2$)
F^{19}	40.055	100	2.6273	1/2	-
Mo^{95}	2.774	15.78	-0.9099	5/2	0.12 ± 0.03 [28]
Mo^{97}	2.833	9.60	-0.9290	5/2	1.1 ± 0.2 [28]
W^{183}	1.75	14.28	0.115	1/2	-

SPIN I = 0 ISOTOPES OF Mo and W

Mo -	I = 0	Mo^{92}, Mo^{94}, Mo^{96}, Mo^{98}, Mo^{100}
W	I = 0	W^{180}, W^{182}, W^{184}, W^{186}

Reference: Handbook of Chemistry and Physics. 48th Edition.

TABLE 2

F^{19} FULL PEAK WIDTH FACTORS FROM Mo^{97} QUADRUPOLAR RELAXATION

$1/Tx10^{+3}$ (K^{-1})	α_1 (hz)	α_2 (hz)	α_3 (hz)	α Average (hz)	α Average x20 (hz)
3.39	0.626	0.392	0.567	0.562	11.24
3.36	0.70	0.361	0.508	0.503	10.46
3.30	0.569	0.396	0.564	0.519	10.38
3.24	0.60	0.376	0.564	0.513	10.26
3.22	0.553	0.341	0.525	0.473	9.46
3.17	0.543	0.354	0.486	0.461	9.22
3.09	0.506	0.341	0.486	0.444	8.88
3.05	0.526	0.326	0.444	0.432	8.64
3.00	0.5	0.497	0.302	0.433	8.66
2.94	0.497	0.313	0.433	0.413	8.26
2.91	0.484	0.322	0.430	0.412	8.24

TABLE 3

CALCULATED PEAK WIDTHS AT HALF-HEIGHT FOR $Mo^{95}F_6$ QUADRUPOLE

$1/Tx10^{+3}$ K^{-1}	15 α (hz)	23 α (hz)	18 α (hz)
3.39	.101	.155	.121
3.36	.0905	.139	.108
3.30	.0933	.144	.112
3.24	.0923	.141	.111
3.22	.0850	.130	.102
3.17	.0830	.127	.0998
3.09	.0814	.124	.0958
3.05	.0775	.119	.0931
3.00	.0780	.1200	.0937
2.94	.0743	.1140	.0892
2.91	.0740	.1135	.0890

TABLE 4

NORMALISED F^{19} FULL PEAK WIDTHS DUE TO Mo^{95} SPIN-ROTATION RELAXATION

$1/Tx10^{+3}$ K^{-1}	R_{1F}(hz)(R+V)	$\Delta\nu_1$ (hz)	$\Delta\nu_2$(hz)	$\Delta\nu_3$(hz)	β (hz)
3.39	0.347	0.90	1.19	1.27	0.028
3.36	0.360	0.92	1.19	1.27	0.027
3.30	0.370	0.927	1.27	1.31	0.026
3.24	0.387	0.90	1.22	1.37	0.0334
3.22	0.394	0.936	1.27	1.37	0.0335
3.17	0.408	0.88	1.20	1.30	0.0325
3.09	0.426	0.945	1.30	1.42	0.0372
3.05	0.44	0.88	1.30	1.42	0.041
3.00	0.46	0.956	1.34	1.50	0.0442
2.94	0.487	1.15	1.575	1.72	0.0445
2.91	0.49	1.33	1.85	1.935	0.043

TABLE 5

F^{19} FULL PEAK WIDTHS FROM W^{183} SPIN-ROTATION RELAXATION

$1/Tx10^{+3}$ K^{-1}	$\Delta\nu$ (hz)	$R_2^* + R_{1F}$ (hz)	β (hz)
3.54	0.54	.514	0.026
3.51	0.50	.47	0.030
3.48	0.50	.467	0.033
3.31	0.55	.497	0.053
3.27	0.52	.49	0.030
3.20	0.50	.45	0.050
3.17	0.56	.485	0.055
3.10	0.60	.57	0.030
3.01	0.57	.502	0.068

Figure 1.

VACUUM APPARATUS FOR PURIFICATION OF N.M.R. SAMPLE

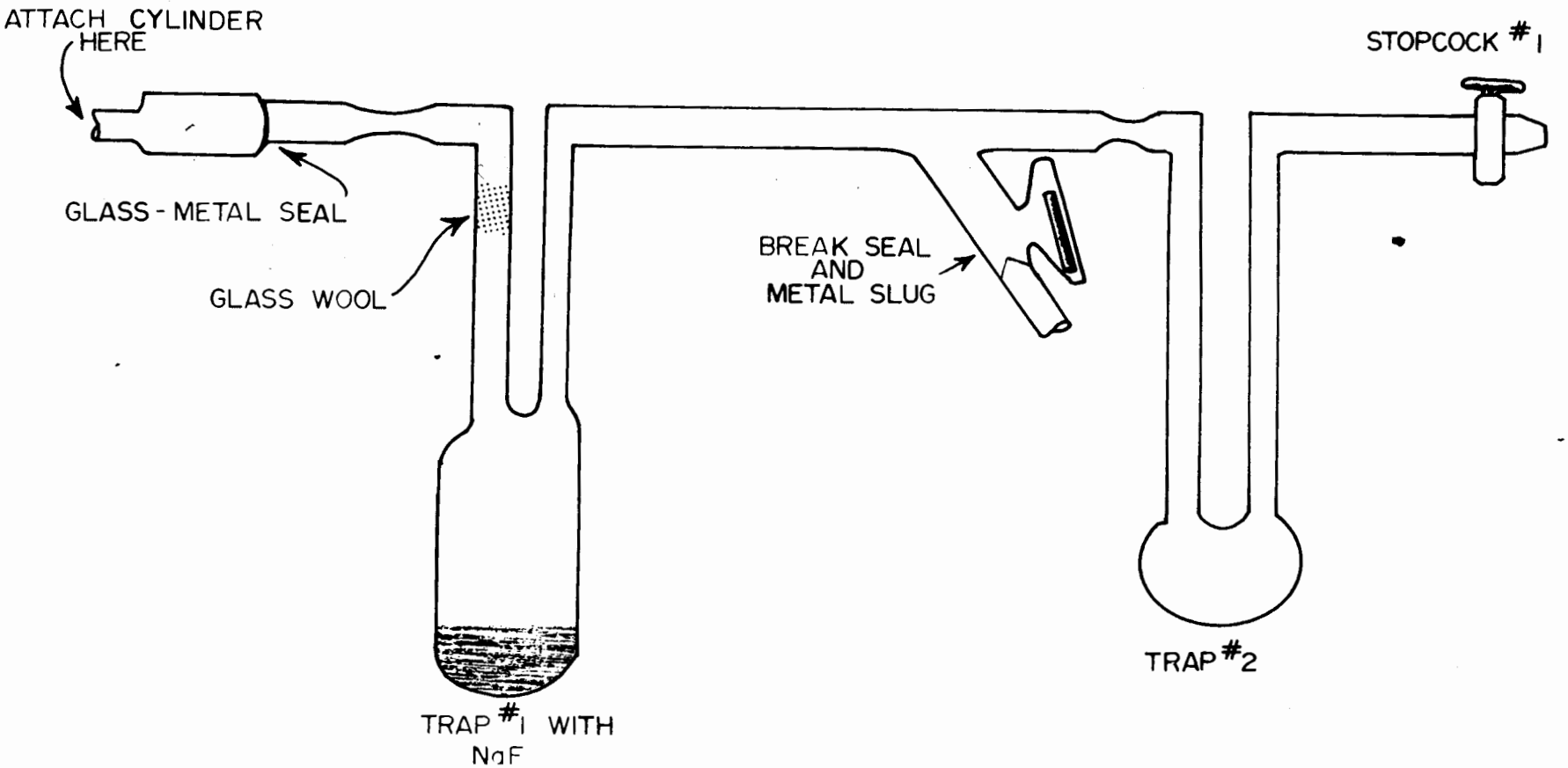
ATTACH CYLINDER HERE
STOPCOCK #1
GLASS - METAL SEAL
GLASS WOOL
BREAK SEAL AND METAL SLUG
TRAP #2
TRAP #1 WITH NaF

Figure 2.

VACUUM APPARATUS FOR TRANSFERRING N.M.R.
SAMPLE TO N.M.R. TUBE

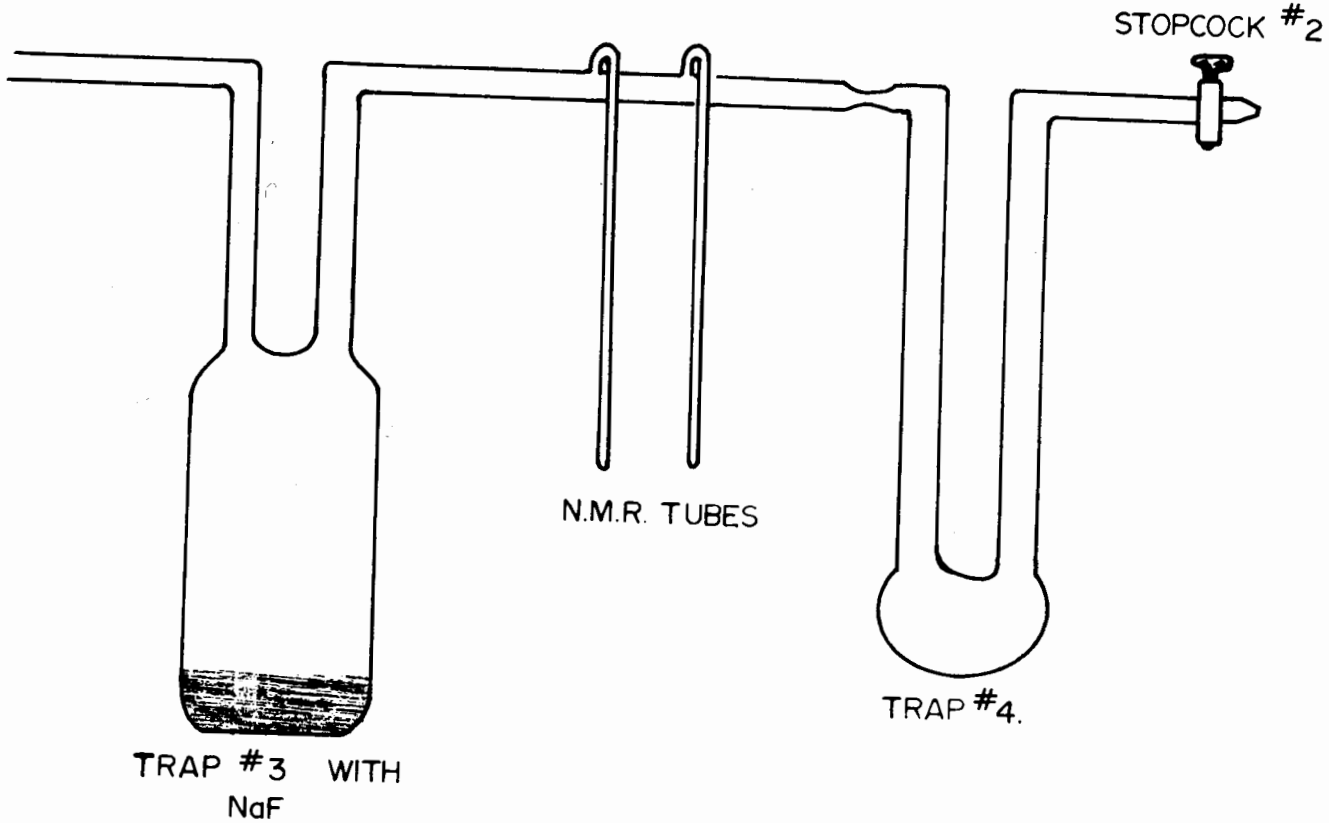
STOPCOCK #2
N.M.R. TUBES
TRAP #4.
TRAP #3 WITH
NaF

Figure 3.

F^{19} SPECTRUM OF MoF_6 AT 33°C

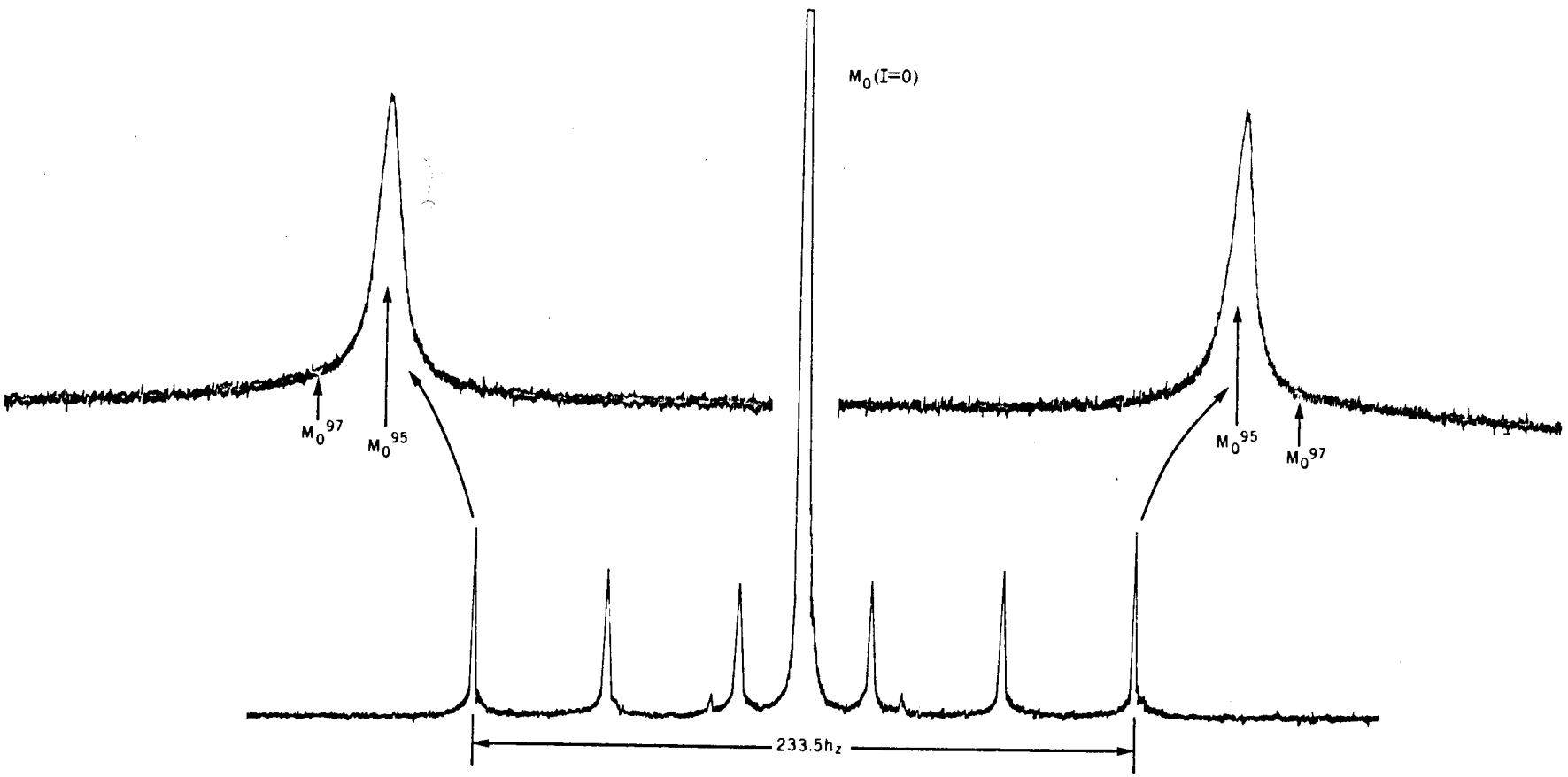
$M_0(I=0)$
M_0^{97}
M_0^{95}
M_0^{95}
M_0^{97}
233.5hz

Figure 4.

F^{19} SPECTRUM OF WF_6 AT 28°C

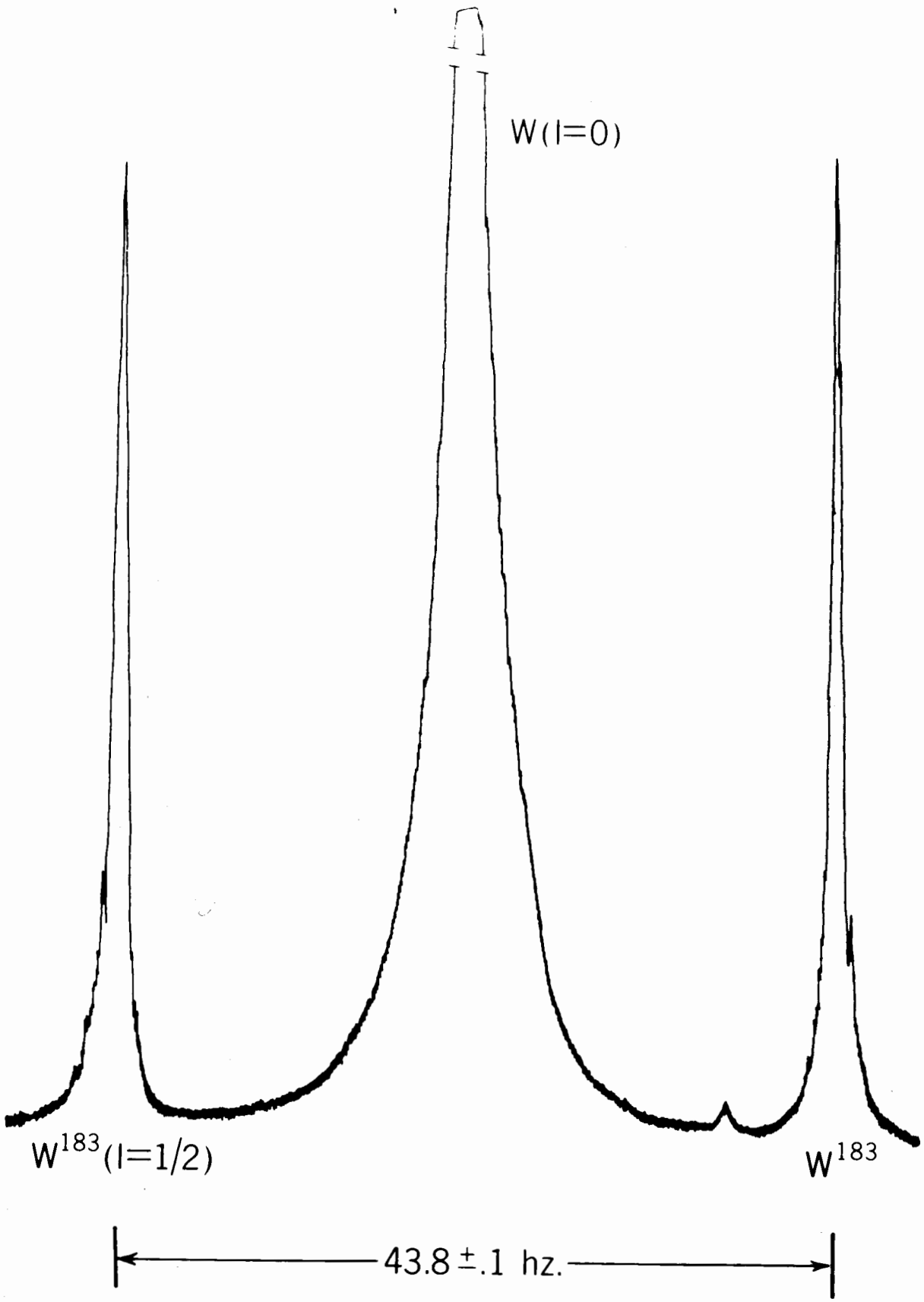
W(I=0)
W183(I=1/2)
W183
43.8 ±.1 hz.

Figure 5.

METHANOL SHIFT VS. TEMPERATURE

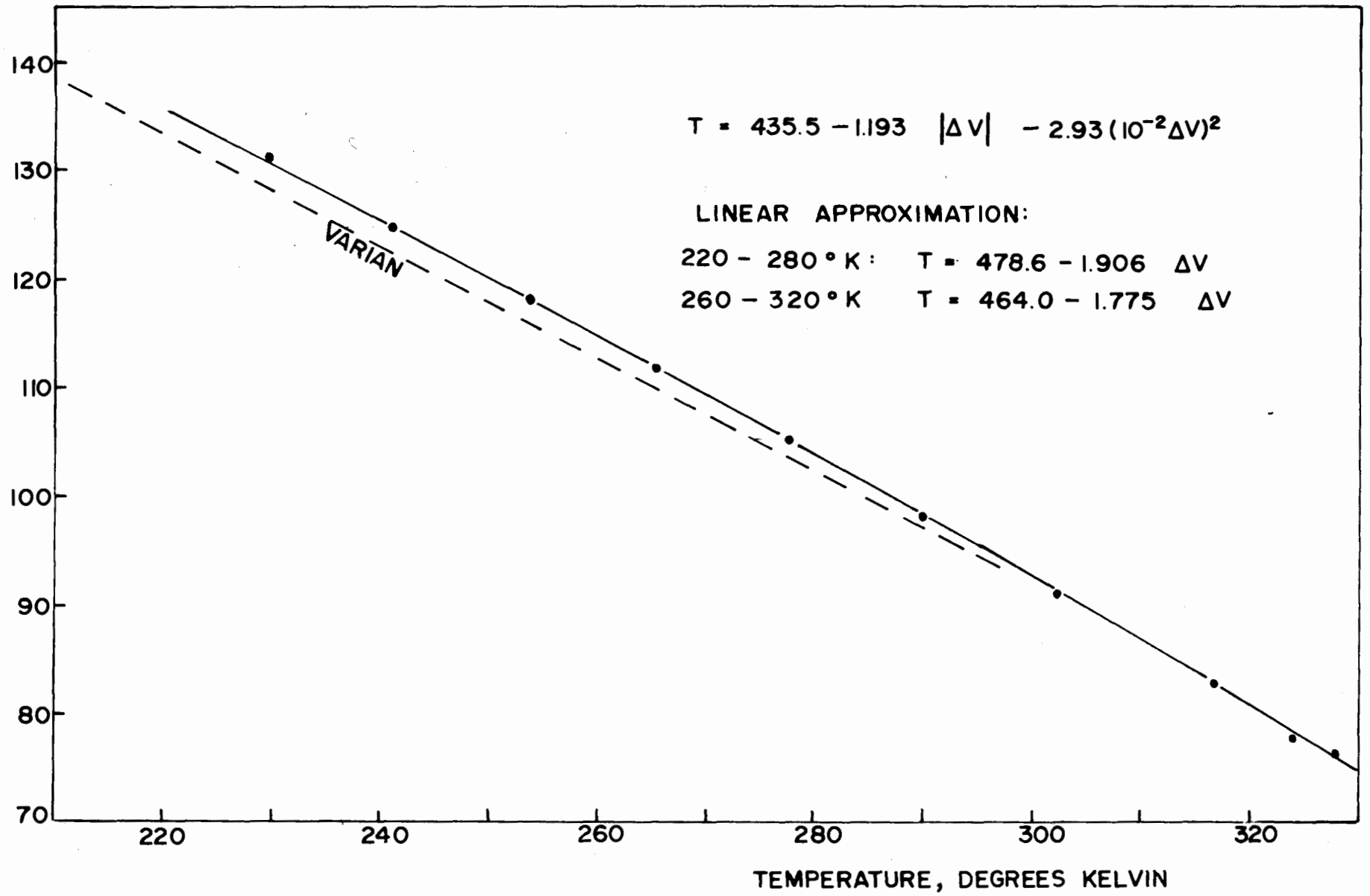
CHEMICAL SHIFT OF METHANOL, HERTZ.
140
130
120
110
100
90
80
70
220
240
260
280
300
320
TEMPERATURE, DEGREES KELVIN
VARIAN
T = 435.5 − 1.193 |ΔV| − 2.93 (10⁻²ΔV)²
LINEAR APPROXIMATION:
220 − 280 °K: T = 478.6 − 1.906 ΔV
260 − 320 °K T = 464.0 − 1.775 ΔV

Figure 6.

ETHYLENE GLYCOL SHIFT VS. TEMPERATURE

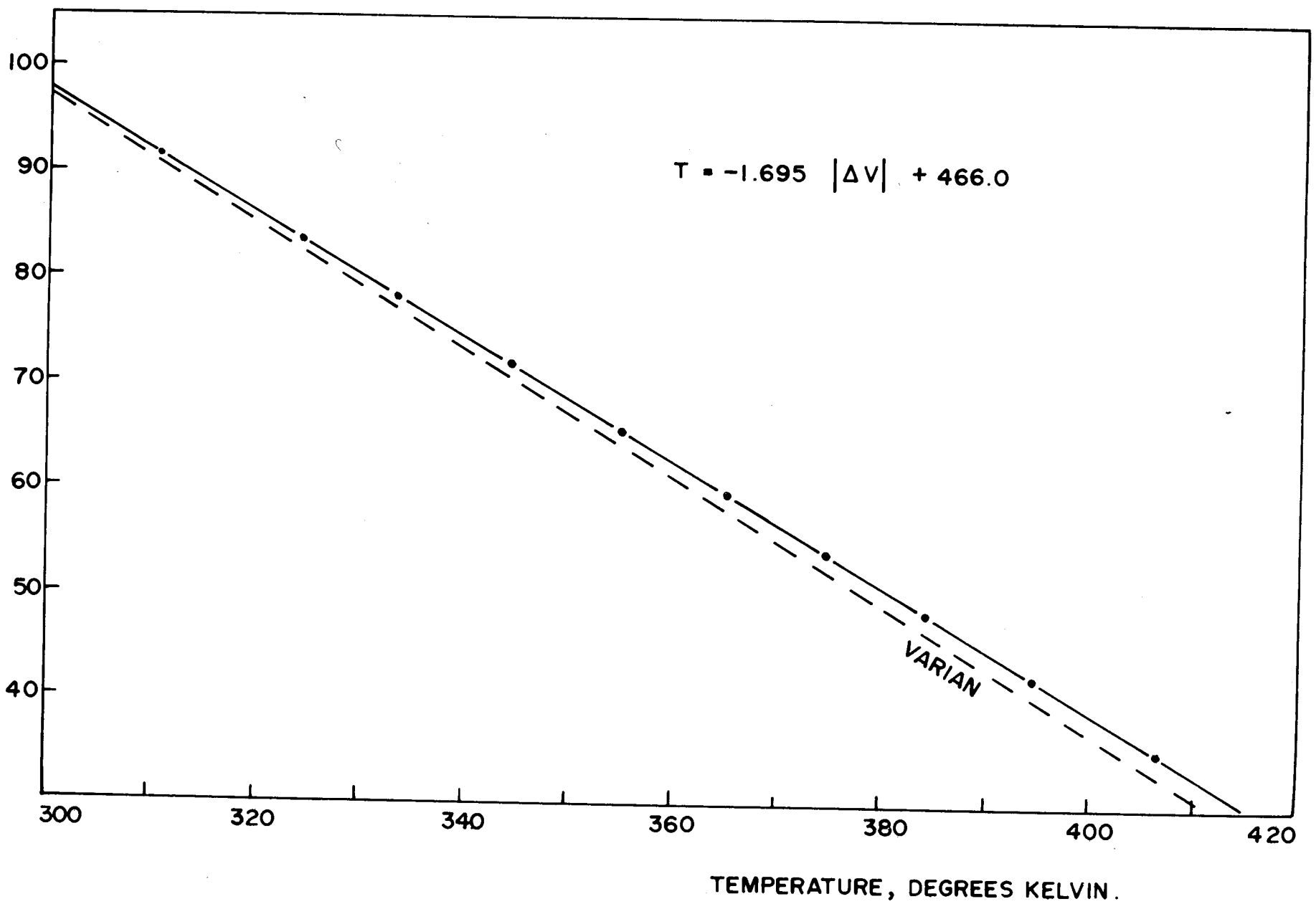
CHEMICAL SHIFT OF GLYCOL, HERTZ.
100
90
80
70
60
50
40
T = -1.695 |ΔV| + 466.0
VARIAN
300
320
340
360
380
400
420
TEMPERATURE, DEGREES KELVIN.

Figure 7.

$\pi - \pi/_2$ PULSE SEQUENCE FOR MoF_6

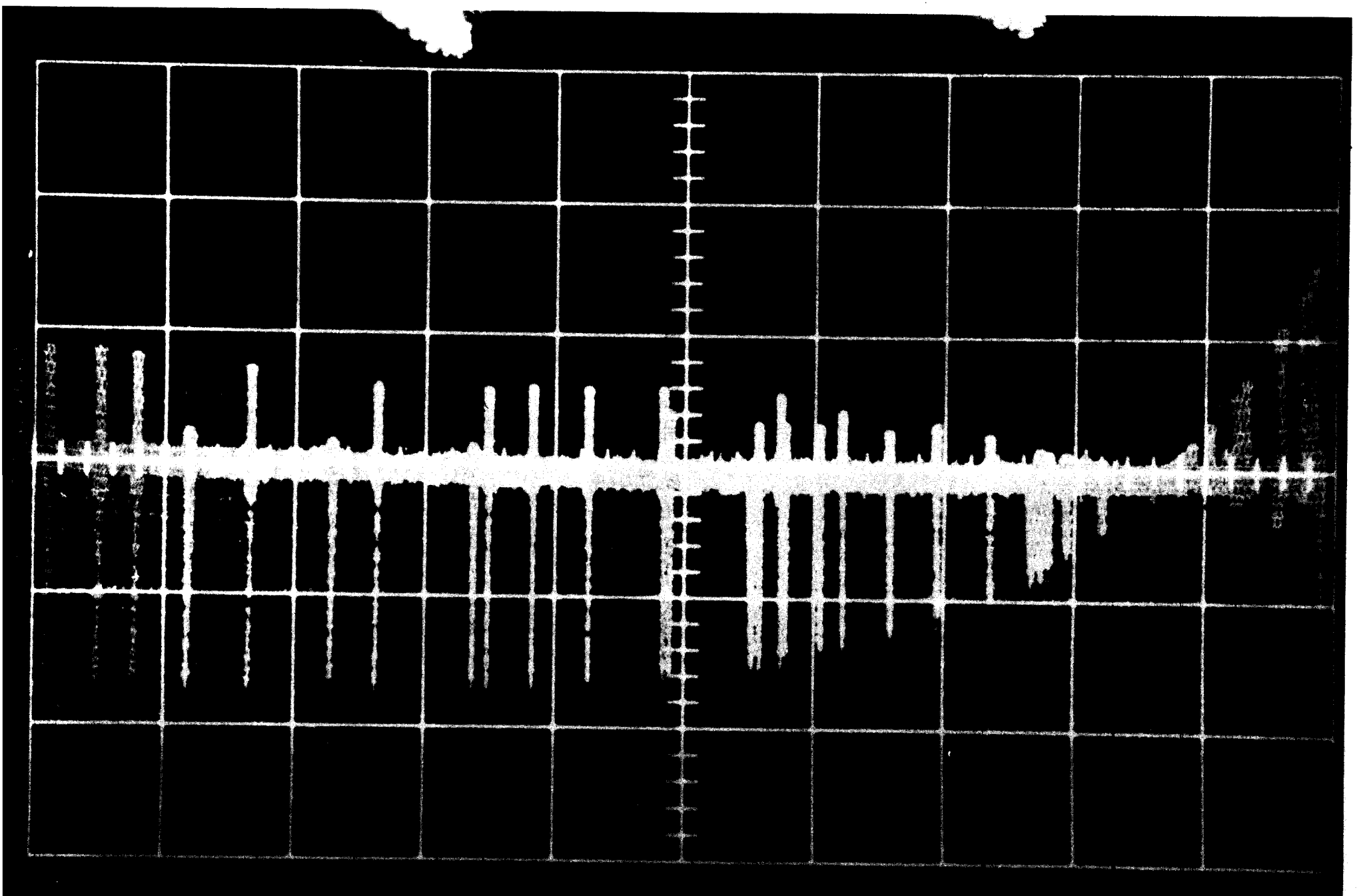

Figure 8.

TIME VS LOG_{10} PEAK HEIGHT FOR $\pi - \pi/2$ PULSE EXPERIMENT

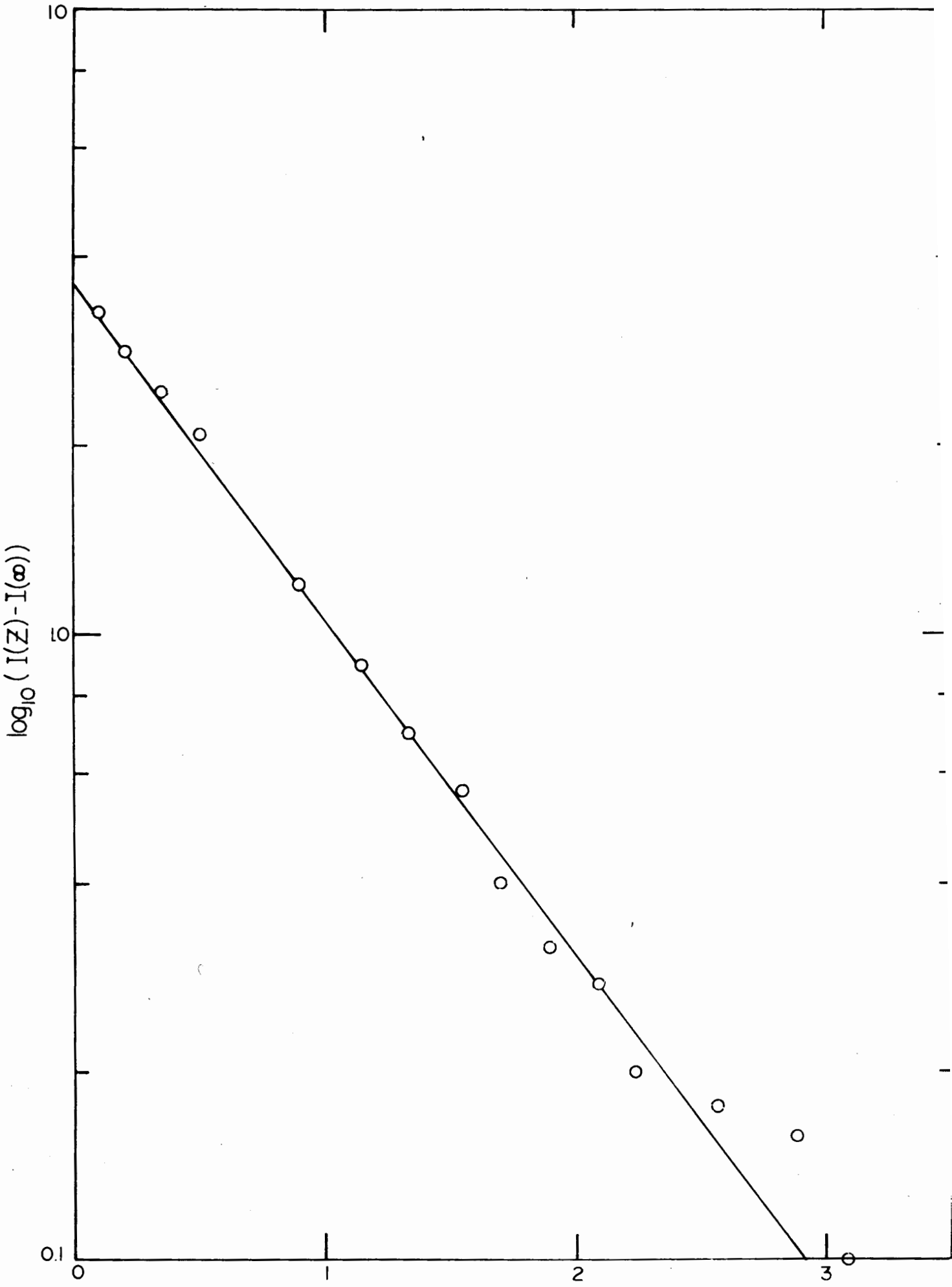
10
1.0
0.1
0
1
2
3
$\log_{10}(I(Z)-I(\infty))$
TIME (sec)

Figure 9.

TEMPERATURE DEPENDENCE OF Mo^{97} AND Mo^{95} RELAXATION MECHANISMS FROM F^{19} SPECTRA
FOR COMPARISON $F^{19}{}_{I.J}$ RELAXATION RATE AND THE F^{19} SPIN DIFFUSION DATA OF RIGNY AND VIRLET (24) ARE ALSO PLOTTED

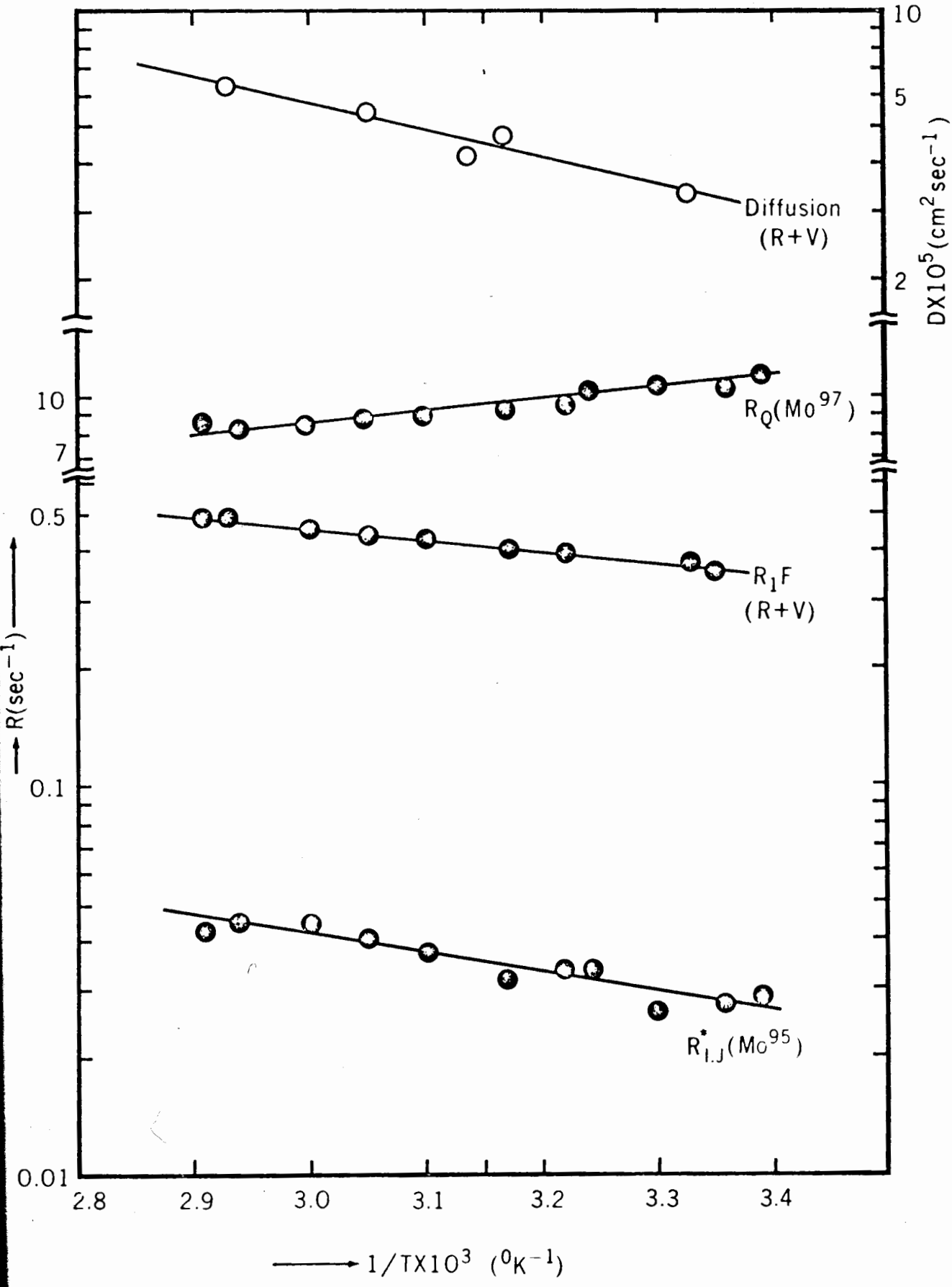
10
5
2
DX10^5(cm^2 sec^-1)
Diffusion
(R+V)
10
7
0.5
0.1
0.01
R(sec^-1)
R_Q(Mo^97)
R_1F
(R+V)
R*_I.J(Mo^95)
2.8
2.9
3.0
3.1
3.2
3.3
3.4
1/TX10^3 (^0K^-1)

Figure 10.

WIGGLE BEAT DECAY CENTRAL PEAK OF WF_6
WHEN DETUNED AT 27°C.
(2 seconds full width)

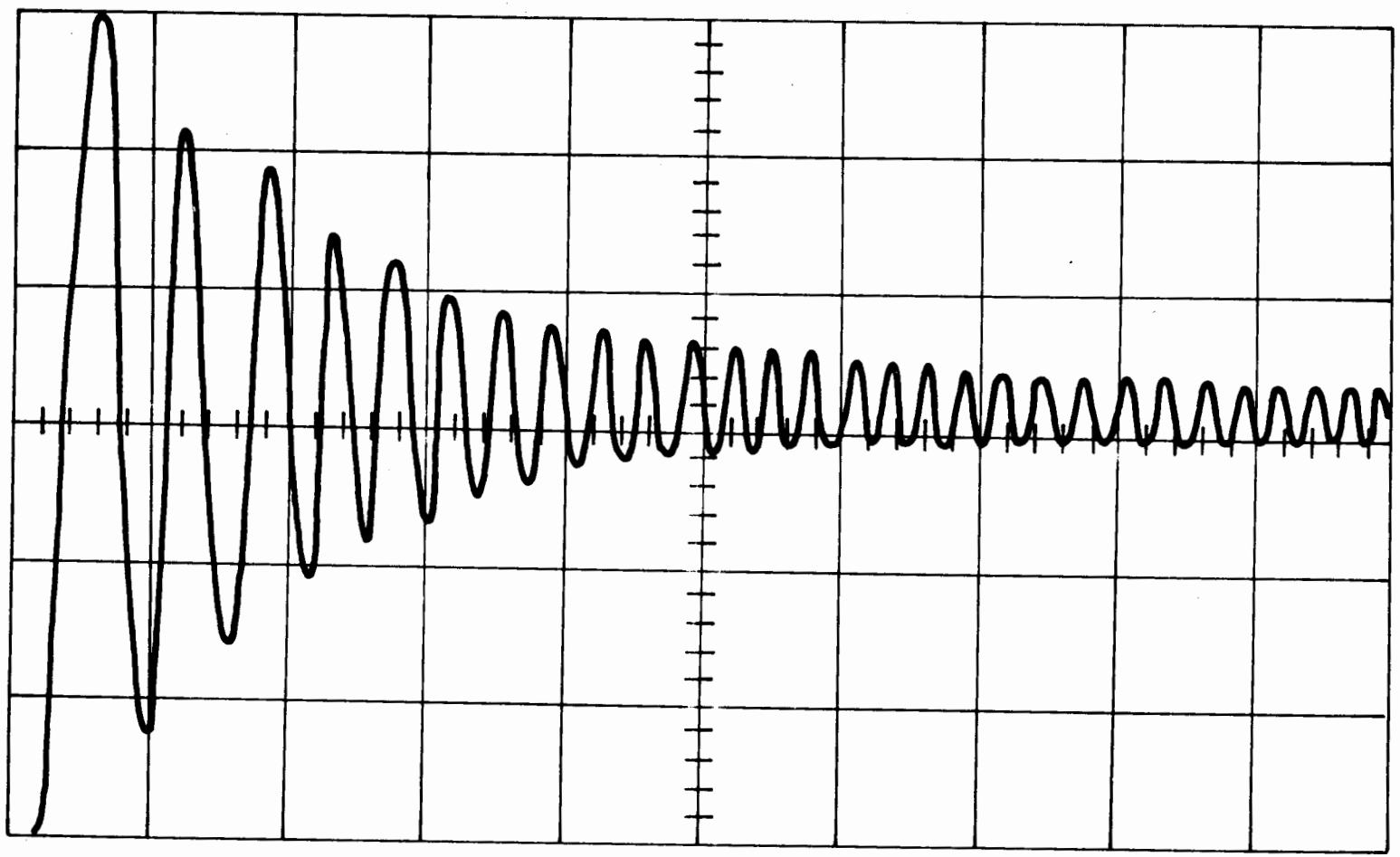

Figure 11.

TEMPERATURE DEPENDENCE OF W^{183} RELAXATION FROM F^{19} SPECTRA
FOR COMPARISON $F^{19}{}_{I.J}$ RELAXATION RATE
AND F^{19} SPIN DIFFUSION DATA OF (R+V) (24) ARE ALSO PLOTTED

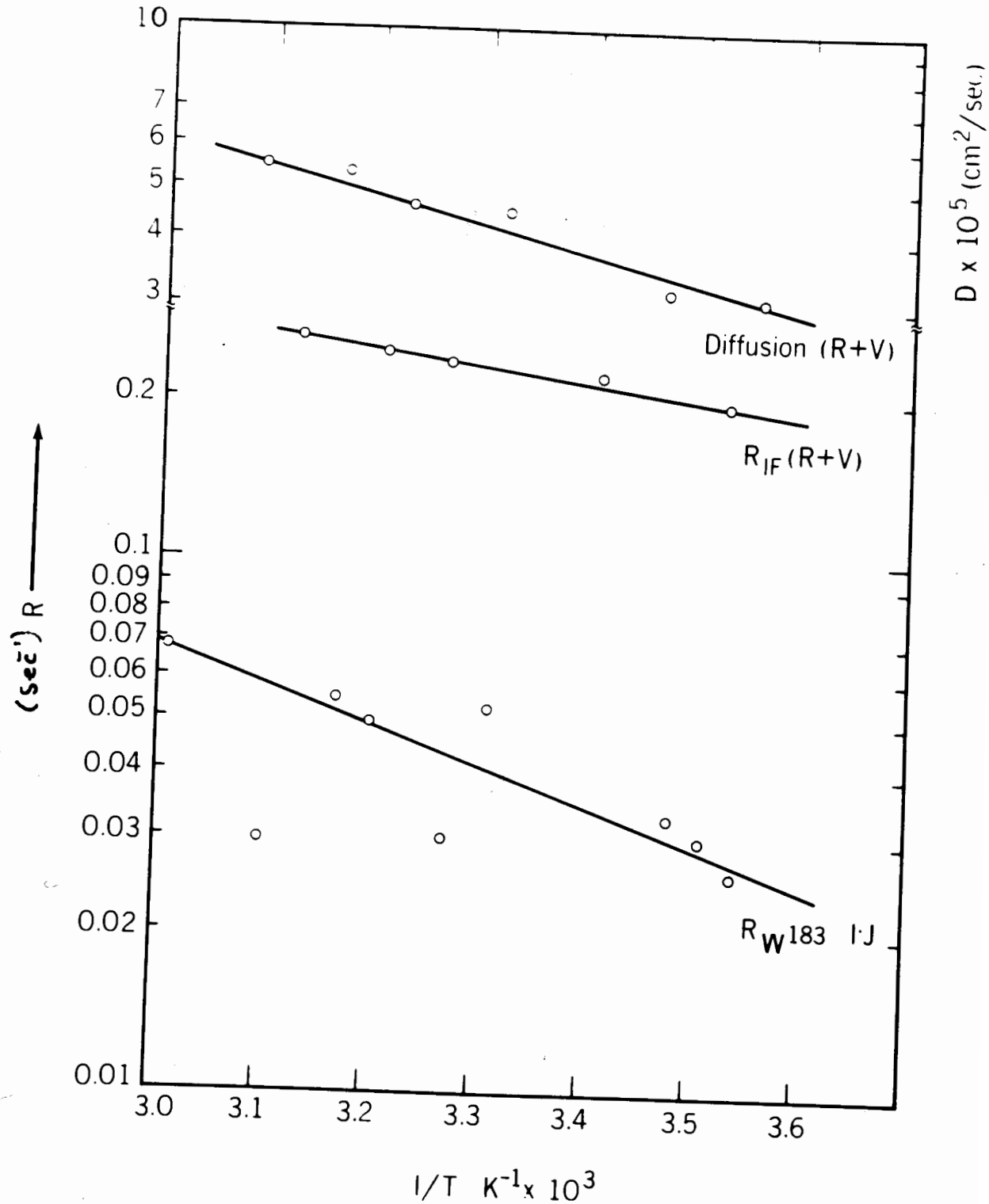
10
7
6
5
4
3
0.2
0.1
0.09
0.08
0.07
0.06
0.05
0.04
0.03
0.02
0.01
3.0
3.1
3.2
3.3
3.4
3.5
3.6
Diffusion (R+V)
R_{IF} (R+V)
R_{W183} I·J
(sec⁻¹) R
D x 10^5 (cm^2/sec.)
1/T K^{-1} x 10^3

CHAPTER V

P.M.R. STUDY OF DEUTERATED AMMONIUM IONS

(1) Introduction

An attempt was made to study the N^{14} relaxation mechanism by rotary echo (1) experiments on the H^1 spectra in aqueous solutions of acidified ammonium ions as a function of temperature.

To perform such an experiment it was necessary to satisfy two conditions. Firstly a solvent had to be obtained in which the ammonium salt was very soluble. Secondly, as pointed out by Ogg (2, 3), those processes of rapid chemical exchange occurring in aqueous solutions of the ammonium ion, shown in section (2) of this chapter, had to be 'frozen' to obtain a well resolved triplet ($I_{N^{14}} = 1$). It was thought that an acidified solution of D_2O would satisfy the above conditions. However, the H^1 spectrum of this sample, run at 60 Mhz, yielded in addition to the expected triplet, fine structure on each member of this triplet. The splitting of the triplet into sub multiplets was further associated with the set of deuterated ammonium isotopes.

A rotary echo experiment was performed on an aqueous acidified sample of ammonium nitrate. Since relaxation was observed to be very fast it became instrumentally impractical

to study the relaxation mechanism of N^{14} by this technique. However, it did seem necessary to prepare solutions of deuterated ammonium ions with varying ratios of the deuterated components thus allowing for a study of the successive deuterium isotope shift in these ions using P.M.R. techniques.

(2) Chemistry of Aqueous Ammonium Ions

It is well known (2, 3, 4, 5) that aqueous solutions of ammonium ions undergo a double exchange process as a function of pH i.e.

$$pH\rangle 2.5 \quad [NH_3H^*]^+ + HOH \rightleftharpoons [NH_4]^+ + HOH^* \qquad (1)$$

$$pH\rangle 1.0 \quad [NH_3H^*]^+ + [NH_4]^+ \rightleftharpoons [NH_4]^+ + [NH_3H^*]^+ \qquad (2)$$

Thus when crystalline ammonium salts are dissolved in 'neutral' D_2O, there is rapid equilibration of the protons among all available sites of all possible deuterated ammonium ions and solvent species. This phenomenon (6, 7, 8) has been used to prepare the complete sequence of deuterated ions to investigate isotope effects on the gross $J_{N^{14}H}$ coupling in the proton spectra.

It will be shown that by quenching both equilibria (1) and (2), by reducing the pH, and by reducing the temperature to $15^{\circ}C$ it becomes possible to resolve the smaller J_{D-N-H} coupling for each species of the completely deuterated sequence, in spite of the residual quadrupole relaxation at the N^{14} and D^2 centres.

(3) Experimental

One of the samples of deuterated ammonium nitrate used in these experiments was prepared by dissolving 1.50 gms of reagent grade ammonium nitrate (The Nichol's Chemical Company Ltd. -98-100% pure) in 0.905 mls of D_2O (Stohler Isotope Chemicals 99.8% D^2) yielding a well resolved spectrum (i.e., showing well resolved submultiplets associated with $\dot{N}H_4$, $\dot{N}H_3D$, $\dot{N}H_2D_2$, $\dot{N}HD_3$). On dissolution the rapid equilibration processes (1) and (2) were found to take forty-five minutes at room temperature, at which time four drops of concentrated nitric acid (Allied Chemical, Canada 70%) were added to 'freeze' these processes. The sample was then placed in a 5 mm O.D.N.M.R. tube and degassed by conventional techniques before being sealed in vacuo.

The H^1 spectrum was obtained at 15°C on a Varian Associates A56/60 spectrometer at 60 Mhz and a sweep rate of 0.05 hz sec^{-1}; with the radio frequency field H_1 set at 0.01 mgauss and filter band width of 2 hz and spectrum amptitude of 20.

The water peak which occurs at high field of the ammonium ion triplet was used as a means of laying side bands on each peak ($\dot{N}H_4$) of the triplet. The splittings thus observed were obtained using a Hewlett-Packard 3300 A function generator connected to a Model 201 B frequency period counter which was in turn connected to the spectrometer.

(4) Results and Discussion

The results obtained in an analysis of the P.M.R. spectra, at 15°C, are given in Table 1. This table indicates that J_{N-H} decreases slightly on deuteration while J_{HND} increases on deuteration; a successive decrease in the chemical shift was also observed on deuteration, all values being taken relative to the peak attributed to the $\dot{N}H_4$ ion.

To interpret the H^1 spectra reference was made to the central peak of the $\dot{N}H_4$ triplet (Fig. 1). Figure 1 also shows an analysis of the submultiplets giving rise to this 'spectrum', arising from the various deuterated components ($\dot{N}H_4$, $\dot{N}H_3D$, $\dot{N}H_2D_2$, $\dot{N}HD_3$) of the ammonium ion. This figure also contains the relative intensities of each member of these submultiplets, calculated by the usual vector addition manner for equivalent spin 1 particles i.e., for $\dot{N}H_3D$ triplets of relative intensity 1 : 1 : 1, for $\dot{N}H_2D_2$ quintets of intensity 1 : 2 : 3 : 2 : 1 and for $\dot{N}HD_3$ septets of the form 1 : 3 : 6 : 7 : 6 : 3 : 1. However, the spectra are not sufficiently well resolved to allow measurement of the expected line width differences between the component multiplets under deuterium quadrupole relaxation.

The observed decrease in J_{N-H} or increase in J_{D-N-H} on deuteration may be explained (9) through a decrease in the bond angle HND due to a decrease in the librational amplitude of the N-D bending mode against the N-H bending. The argument is to consider a valence bond approach (10) to the ammonium ion and to note how the bond angle H—N—H changes on

deuteration of the ion, attributing any change to a reduction in s-character at the N of the N-H σ-bond, and an overall change in the hybridization of the molecule.

From the ratio D.H = 1/6.53, and Table 1 for values of J_{D-N-H}, it is possible to calculate a theoretical value for J_{H-N-H} if it existed in the same molecular environment as the deuterated species i.e.

	$\overset{+}{N}H_3D$	$\overset{+}{N}H_2D_2$	$\overset{+}{N}HD_3$
J_{H-N-H}	10.46	10.66	11.25

These results were then referred to the Karplus curve (10), suggesting that on deuteration the N^{14} centre undergoes a change in hybridization due to a decrease in the angle H-N-H. The assumption being made that geminal J dependence in the charged $\overset{+}{N}H_{4-n}D_n$ species is similar to that in uncharged methanes.

In comparing our results with those of Fraenkel (11), who obtained a constant value for J_{D-N-H} with a downfield deuterium isotope shift, it was possible to interpret a slight change in the coupling constant J_{D-N-H} by considering differential effects of slow chemical exchange on the various isotopic species.

It is a well known fact that the deuterated ion is more strongly solvated than the non-deuterated ion (12), due to the lower zero point librational frequency of the -X-D-Y- bond against the -X-H-Y- bond. An increase in the structure

about the deuterated molecule causes an increase in the amplitude of librational oscillation and hence a decrease in the kinetic energy of the molecule. Hence in considering the formation of a more efficient H-bond, and by assuming an inductive effect towards the deuterium-hydrogen bond i.e.

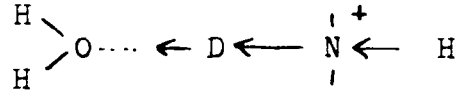

it is possible to account for the observed downfield chemical shift, as due to a decrease in the diamagnetic contribution of the chemical shift at the inductively connected protons. Hence as the ammonium ion becomes progressively more deuterated, the efficiency of the above mechanism should increase, this is in fact borne out by the linear plot Fig. 2.

It is interesting to note that the magnitude of the upfield chemical shift (9) observed by Gutowsky for the sequence of deuterated methanes is of the same magnitude as the downfield shift observed by us; suggesting that this mechanism, which causes a decrease in the diamagnetic shielding constant was twice as large as that associated with an increase in the same constant through the bending vibration effect for an uncharged, solvated molecule of the same apparent symmetry.

Subsequent to our work McFarlane and Dean (13) reported on the heteronuclear double resonance of partially deuterated ammonium bromide. In this report, constant values for J_{D-N-H} and J_{N-H} are given, but a progressive downfield shift on deuteration was attributed to the formation of H-bonds.

BIBLIOGRAPHY

1. E. J. Wells, K. Abramson, J. Mag. Res. To be published.

2. R. A. Ogg, J. D. Ray, Disc. Faraday Soc. 19, 239 (1955).

3. R. A. Ogg, J. D. Ray, J. Chem. Phys. 26, 1339, 1515 (1957).

4. J. Emsley, J. Feeney, L. Sutcliffe, 'High Resolution Nuclear Magnetic Resonance Spectroscopy' (Pergamon Press 1967).

5. H. M. McConnell, D. D. Thompson, J. Chem. Phys., 31, 85 (1959).

6. N. Muller, R. Birkhahn, J. Chem. Phys., 43, 4540 (1965).

7. G. Fraenkel, W. Burlant, J. Chem. Phys., 43, 4541 (1965).

8. R. B. Johanasen, J. Chem. Phys., 48, 1414 (1968).

9. H. S. Gutowsky, J. Chem. Phys., 31, 1683 (1959).

10. H. G. Hecht, 'Magnetic Resonance Spectroscopy' (p. 117) Wiley (1967).

11. G. Fraenkel, Y. Asali, H. Batiz-Hernandex, R. A. Bernheim, J. Chem. Phys., 44, 4647 (1966).

12. C. Gardner Swain, R. Bader, Tetrahedron 10, 182 (1960); Tetrahedron 10, 200 (1960).

13. W. McFarlane, R. Dean, J. Chem. Soc. (A), 1535 (1968).

TABLE I

CHEMICAL SHIFT AND COUPLING CONSTANTS

	NH_4^+	NH_3D^+	$NH_2D_2^+$	NHD_3^+
$J_{N^{14}-H}$ (hz)	52.6 ± 0.2 ($\bar{J}$)	$J-(0.06\pm0.03)$	$J-(0.07\pm0.03)$	$J-(0.08\pm0.03)$
J_{D-N-H} (hz)	-	1.60 ± 0.02	1.63 ± 0.04	1.72 ± 0.02
δ relative NH_4^+ (p.p.m)	0	$-(0.015\pm0.001)$	$-(0.032\pm0.001)$	$-(0.049\pm0.001)$

Figure 1.

CENTRE PEAK OF AMMONIUM ION TRIPLET
SHOWING SUBMULTIPLETS AND ASSIGNMENTS

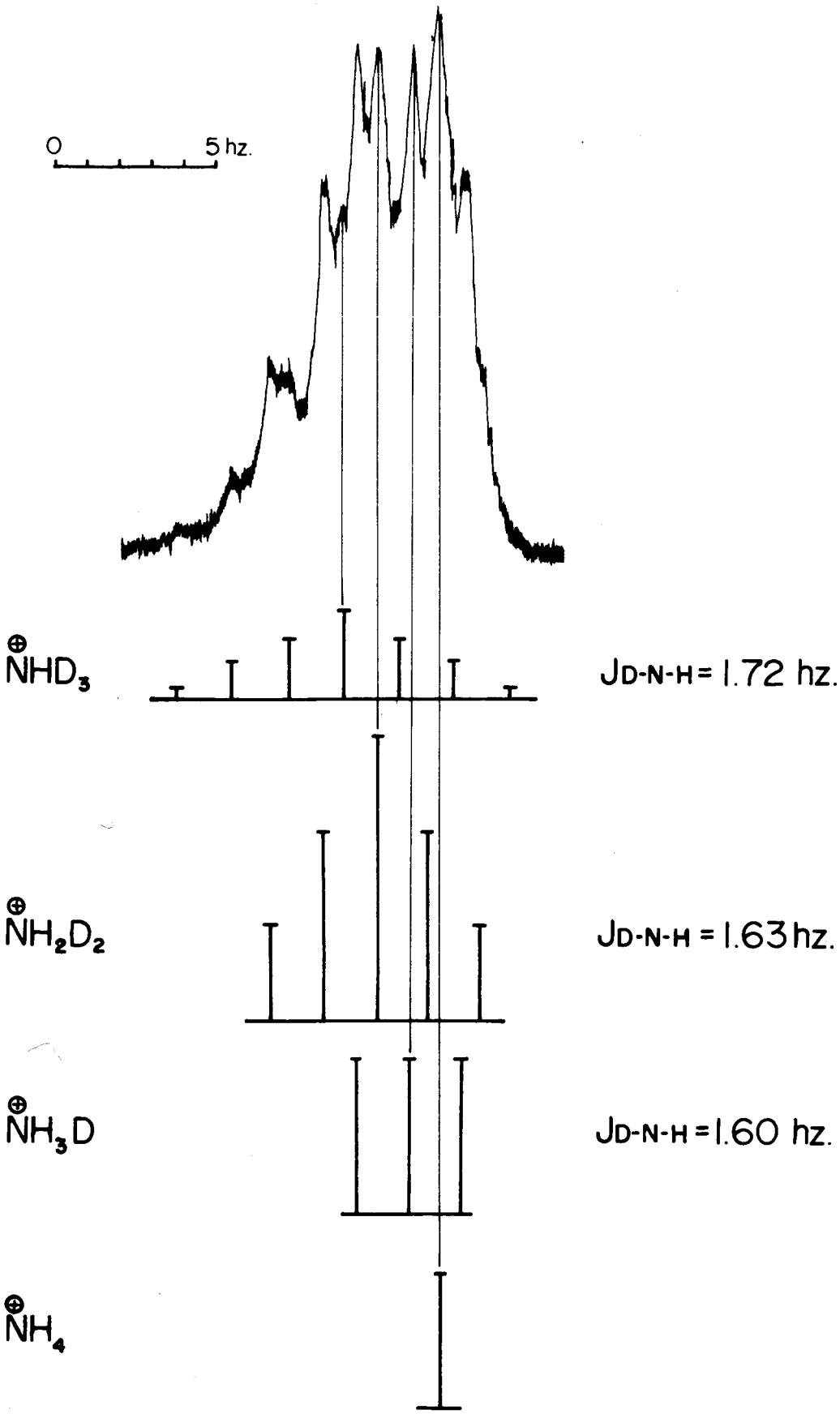
0
5 hz.
$\overset{\oplus}{N}HD_3$
$J_{D\text{-}N\text{-}H}$ = 1.72 hz.
$\overset{\oplus}{N}H_2D_2$
$J_{D\text{-}N\text{-}H}$ = 1.63 hz.
$\overset{\oplus}{N}H_3D$
$J_{D\text{-}N\text{-}H}$ = 1.60 hz.
$\overset{\oplus}{N}H_4$

Figure 2.

CHEMICAL SHIFT (p.p.m.) VS
NUMBER OF HYDROGENS ON THE AMMONIUM ION

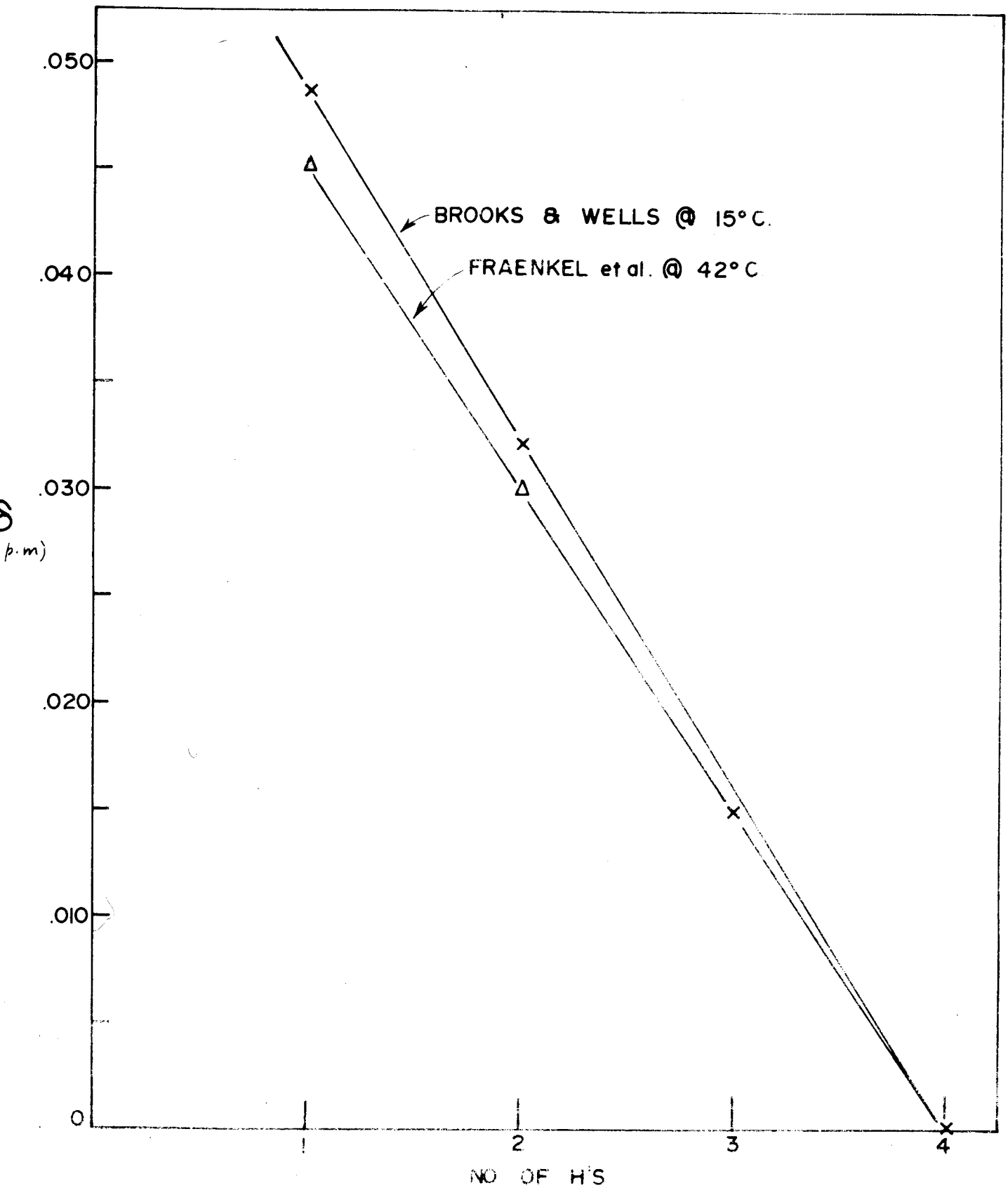
.050
.040
.030
.020
.010
0
BROOKS & WELLS @ 15° C.
FRAENKEL et al. @ 42° C
1
2
3
4
NO OF H'S

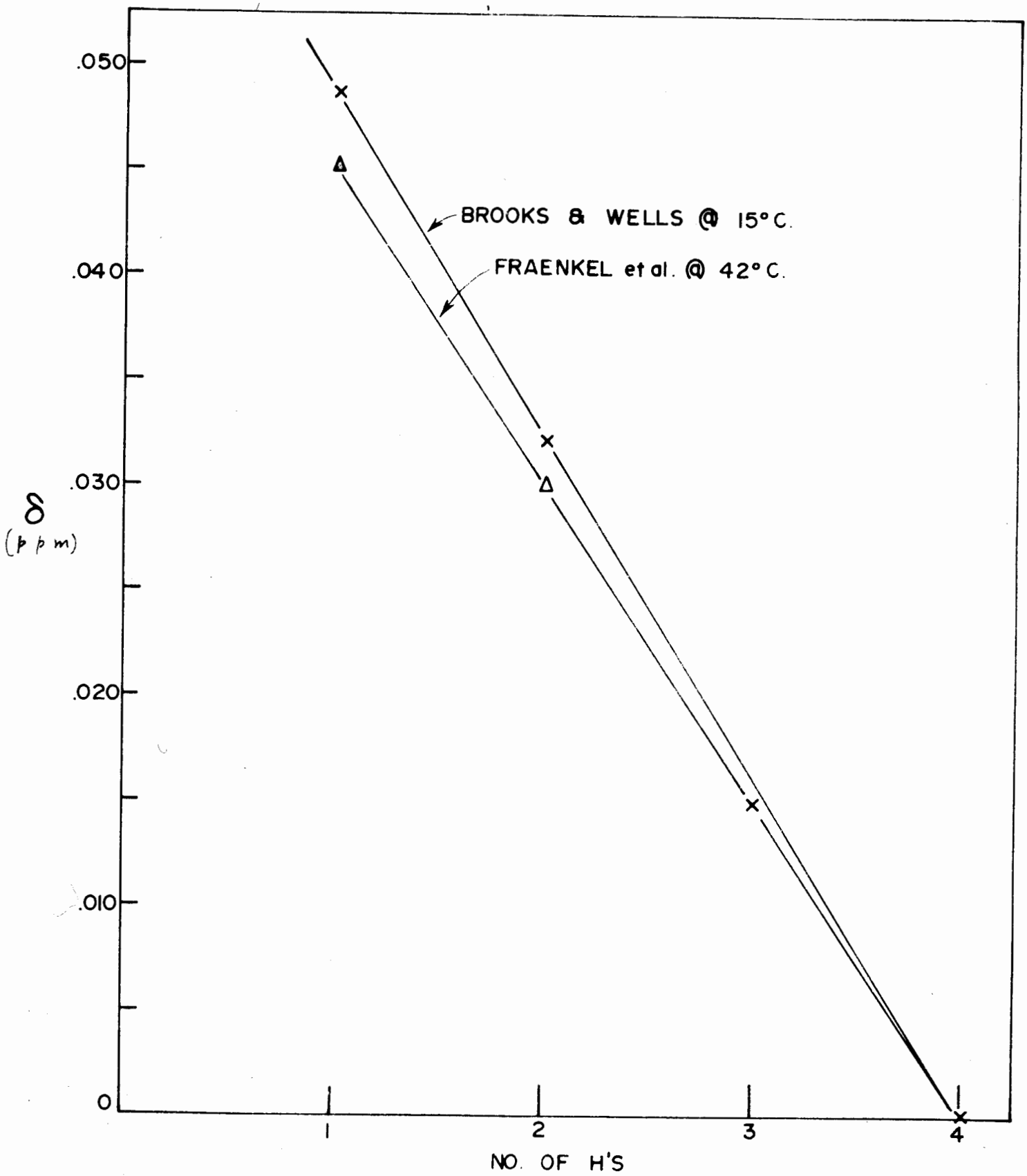
.050
.040
.030
.020
.010
0
δ
(p p m)
BROOKS & WELLS @ 15° C.
FRAENKEL et al. @ 42° C.
1
2
3
4
NO. OF H'S